Journal of Volcanology and Geothermal Research 444 (2023) 107963

Contents lists available at ScienceDirect

Journal of Volcanology and Geothermal Research

journal homepage: www.journals.elsevier.com/journal-of-volcanology-and-geothermal-research

Tectonic-magmatic-hydrothermal interactions in a hot dry rock geothermal system: The role of the transfer and normal faults in the Acoculco caldera (Mexico)

Domenico Liotta [a,b,*], Andrea Brogi [a,b], Walter H. Wheeler [c], Eivind Bastensen [c], Victor Hugo Garduño-Monroy [d], José Luis Macias [e], Giovanni Sosa-Ceballos [e], Antonio Pola [e], Denis-Ramón Avellán [e], Caterina Bianco [a], Emmanuel Olvera-García [d], Fidel Gómez-Alvarez [d], Isabel Israde-Alcantara [d], Adrian Jiménez-Haro [d], Luigi Piccardi [f], Martina Zucchi [a]

[a] Dipartimento di Scienze della Terra e Geoambientali, Università degli studi di Bari Aldo Moro, Bari, Italy
[b] CNR-IGG, Istituto Geoscienze e Georisorse - Consiglio Nazionale delle Ricerche, Pisa, Italy
[c] NORCE Norwegian Research Centre, Bergen, Norway
[d] Instituto de Investigaciones en Ciencias de la Tierra, Universidad Michoacana de San Nicolás de Hidalgo, Morelia, Mexico
[e] Instituto de Geofísica, Universidad Nacional Autónoma de México, Morelia, Mexico
[f] CNR-IGG, Istituto Geoscienze e Georisorse - Consiglio Nazionale delle Ricerche, Firenze, Italy

ARTICLE INFO

Keywords:
Extensional tectonics
Transfer faults
Geothermal system
Acoculco caldera
Mexico

ABSTRACT

In the Acoculco caldera (hot dry rock system) two geothermal boreholes were planned to intersect fracture systems in the carbonate basement. Even though the caldera is located in an area of active deformation with high rainfall, a scarce permeability was recognized. To shed light on this apparent mismatch, we investigate the area by integrating a structural and kinematic dataset on faults and fractures with the volcanological data. The results highlighted two main coeval fault systems, NW- and NE striking respectively, and two associated minor N-S and E-W striking sets, affecting the area of the Acoculco caldera and controlling its volcanic evolution. The kinematic analysis on fault-slip surfaces demonstrated that the NW-striking faults are characterized by two superposed movements: the first comprises right strike-slip to right lateral oblique-slip, while the second is dominantly normal. In contrast, the NE-striking structures display only dominantly normal movements. We explain the kinematic evolution by two recurring events, determined by the interplay between regional extension and uplift: when a crustal extension was dominant in the region (first kinematic event), the NW- and NE-trending structures played the role of transfer and normal faults, respectively; in contrast, when uplift predominated (second kinematic event) both the pre-existing NW- and NE-striking faults acted with normal movements. The location of eruptive centers is controlled by the permeability along the regional faults and their step-over zones. A closer analysis carried out in the surroundings of the geothermal boreholes suggests that deformation migrated northwards, and that fractures are sealed in this sector of Acoculco, thus strongly reducing permeability. In this view, the most promising areas for potential permeability at depth might occur northwards, beyond of the Acoculco caldera, and along the NW-trending structures. In conclusion, the fault kinematics is influenced by periods of increased partial melting of the lithosphere, the latter determining anomalous heat flux and uplift. This process interacts with the fluid pathways that are in turn controlled by the tectonic segmentation, and this is a new model to explain the tectonic-magmatic and hydrothermal interaction of this region.

1. Introduction

Active natural geothermal systems are linked to the contemporaneous occurrence of three main factors: infiltration of meteoric waters, rock permeability, and natural heat flux, generally >80 mW/m^2 (Barbier, 2002). When one of these main factors is absent, the natural geothermal system is not entirely developed. In this view, central Mexico (i.e., the Trans-Mexican Volcanic Belt) is one of the most

* Corresponding author at: Dipartimento di Scienze della Terra e Geoambientali, Università degli studi di Bari Aldo Moro, Bari, Italy.
E-mail address: domenico.liotta@uniba.it (D. Liotta).

https://doi.org/10.1016/j.jvolgeores.2023.107963
Received 18 February 2023; Received in revised form 21 October 2023; Accepted 7 November 2023
Available online 10 November 2023

favorable areas in the world in terms of geothermal potentiality with local heat flux peaks >200 mW/m^2 (e.g., Prol-Ledesma and Morán-Zenteno, 2019). One of these sites is located in the area around the Acoculco village, nearby the Los Humeros active geothermal field (Fig. 1). Here, the thermal gradient is up to 150 °C per km (Lopez-Hernandez and Castillo-Hernandez, 1997), and abundant rainfall is occurring during the seasonal rain period (up to 500 mm/m^2, Vega et al., 2014).

The rock succession is primarily represented by volcanic and sedimentary deposits related to the late Pliocene caldera collapse, and Pleistocene post-caldera deposits resting over Miocene to Pliocene volcanic rocks (13–3 Ma), lying on a pre-volcanic substratum made up of Cretaceous limestone (De la Cruz and Castillo-Hernández, 1986; López-Hernández and Martínez, 1996; Avellán et al., 2019; Avellán et al., 2020). The latter was affected by contact metamorphism and metasomatism during the cooling of a Pliocene-Pleistocene granitoids (Gutiérrez-Negrín, 2013), laccoliths and swarms of dikes-and sills (Avellán et al., 2020).

Despite favorable values of heat flux and rainfall, permeability appears to be insufficient to allow geothermal fluid flow (Viggiano-Guerra et al., 2011; Gutiérrez-Negrín, 2013): this is suggested by two unsuccessful exploration geothermal boreholes drilled near a CO_2 bubbling swamp area (Polak et al., 1982; Quinto et al., 1995; López-Hernández et al., 2009). Hydraulic tests in the borehole indicated very low permeability values, thus suggesting possible sealing of fractures by hydrothermal minerals (López-Hernández et al., 2009).

Nevertheless, the area is affected by intense brittle deformation framed in the active NW-oriented regional stretching (Lermo-Samaniego and Bernal-Esquia, 2006; García-Palomo et al., 2018; Sosa-Ceballos et al., 2018; Avellán et al., 2020; Olvera-García et al., 2020; Avellán et al., 2020) determining two main fault systems, NW- and NE-striking respectively (García-Palomo et al., 2018; Avellán et al., 2020). In this setting, enhanced fracture-related permeability proximal to fault zones would be expected (e.g., Seebeck et al., 2014), especially, if faulting is recent and still active. Thus, the lack of sufficient permeability in the exploration wells is an apparent paradox.

This paper considers the distribution of faults to improve our understanding of their influence on permeability within accessible crust (Curewitz and Karson, 1997; Sibson, 2000; Rowland and Sibson, 2004; Seebeck et al., 2014; Fossen and Rotevatn, 2016). We present a kinematic analysis of fault-slip surfaces and derive the intermediate stress axis, which controls the distribution of permeability in fault systems (Fig. 2).

2. Geological setting

During late Cretaceous-Miocene, the Jurassic-Cretaceous sedimentary basement, mainly composed of carbonate deposits, was affected by the Laramide orogeny during which a thrust and fold belt with a NE vergence developed under a NE-SW oriented tectonic transport direction (Suter, 1987; Sedlock et al., 1993; Eguiluz de Antuñano et al., 2000; Padilla-Sanchez, 2007; Chavez-Ceballos et al., 2011; Cuéllar-Cárdenas et al., 2012; Fitz-Díaz et al., 2012; Fitz-Diaz et al., 2014). The eastern sector of the Trans-Mexican Volcanic Belt (TMVB) was then affected by magmatism since middle Miocene, which evolved in time and space through to the Holocene (Demant and Robin, 1975; Pasquaré et al., 1991; Suter, 1991; Garduño-Monroy and Gutiérrez-Negrín, 1992; Garduño-Monroy et al., 1993; Hasenaka, 1994; Ferrari et al., 1999; Ferrari et al., 2000; García-Palomo et al., 2000; García-Palomo et al., 2002a, 2002b; Gómez-Tuena et al., 2005; Ferrari et al., 2011; Gómez-Vasconcelos et al., 2015).

The TMVB derives from a continuous, mainly calc-alkaline, volcanic activity, associated with the subduction of the Cocos Plate underneath the North America Plate, along the Pacific margin (Pasquaré et al., 1991; Suter et al., 2001; Gómez-Tuena et al., 2005). This scenario, characterized by a Pliocene to Present mainly NW-SE trending extension (Pasquaré et al., 1988; Suter et al., 2001; Ego and Ansan, 2002), overprinted a previous extensional tectonic setting, active from middle Miocene to early Pliocene and giving rise to the southern termination of the Basin and Range fault system of western North-America plate, developed under a mainly ENE-trending extension (Pasquaré et al., 1988). Tectonic activity in the central sector of the TMVB is indicated by

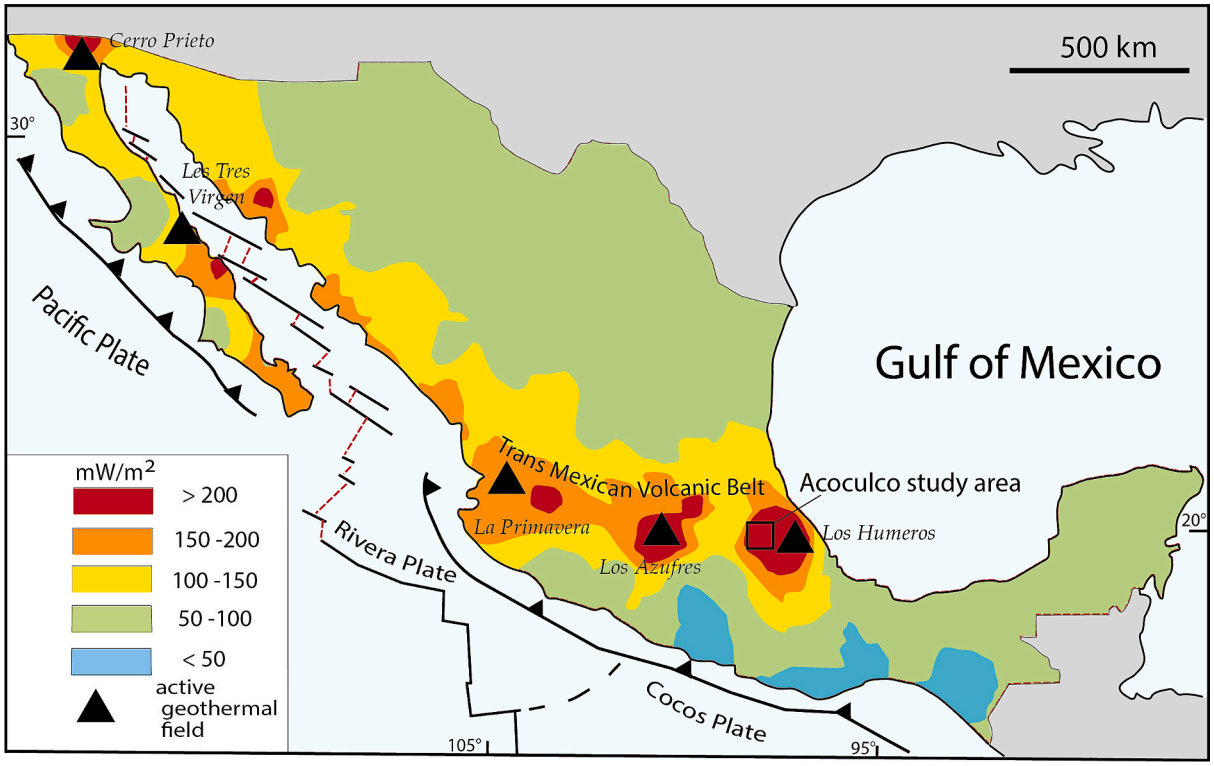

Fig. 1. Simplified heat flow map of Mexico (after Prol-Ledesma and Morán-Zenteno, 2019).

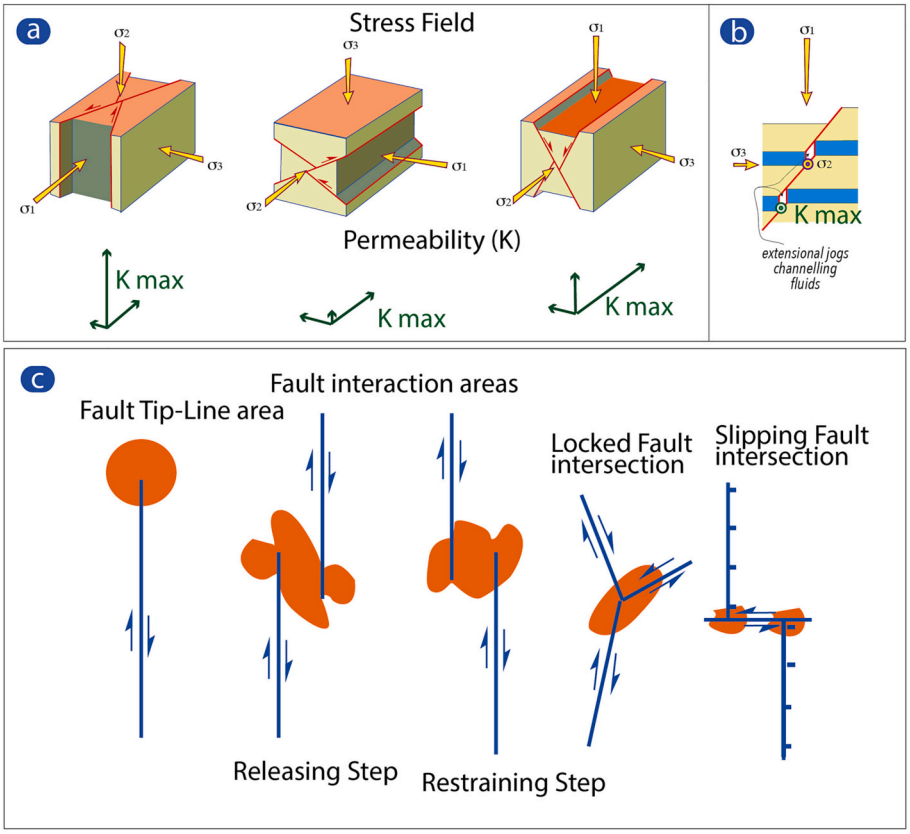

Fig. 2. a) Relationships between the main stress axes in the Andersonian theory and direction along which permeability (K) is favored (after Faulkner and Armitage, 2013); b) sketch illustrating the relationships between permeability and stress axes, in a normal fault developing extensional jogs (after Sibson, 2000): the same relation is envisaged for strike- slip and reverse faults, although the latter are the less favorable to fluid flow; c) areas of enhanced permeability associated to fault segments and their cross-cutting relations (after Curewitz and Karson, 1997).

widespread seismicity and earthquakes ($M \leq 5$) with focal mechanisms ranging from transcurrent to normal (Quintanar et al., 2004; Quintanar et al., 2018; Suárez et al., 2019; Córdoba-Montiel et al., 2023).

The Acoculco Caldera is located at the intersection of two regional fault systems, one NE-striking and the other NW-striking (López-Hernández et al., 2009), respectively interpreted as normal and transfer faults (Pérez-Orozco et al., 2021). According to Avellán et al. (2019) and Avellán et al. (2020), the units associated with the Acoculco Caldera are grouped into four eruptive phases of volcanism (Fig. 3): *syn*-caldera, early post-caldera, late post-caldera, and extra-caldera. The syn-caldera phase correlates to the collapse and formation of the Acoculco caldera, which produced the Acoculco andesitic ignimbrite, about 2.7 Ma (Avellán et al., 2019; Avellán et al., 2020). This collapse determined a caldera 18 by 16 km in areal dimension, and the establishment of an intra caldera lake, filled with lacustrine sediments (Avellán et al., 2020). Subsequently, a first post-caldera eruptive phase occurred, dominantly inside the caldera, between 2.6 and 2.1 Ma. This event was defined as early post-caldera volcanism (Avellán et al., 2020). It produced lava flows and domes dominantly of basaltic trachyandesite to basaltic composition (Sosa-Ceballos et al., 2018; Avellán et al., 2020). Afterwards, a second post-caldera phase took place along the caldera margins, emplacing rhyolitic lava domes, lava flows and two younger ignimbrites, between 2.0 Ma and < 16 ka. These latter were established in the late post-caldera phase (Sosa-Ceballos et al., 2018; Avellán et al., 2019; Avellán et al., 2020). Finally, the fourth eruptive phase, known as extra-caldera volcanism, is directly related to the establishment of the Apan-Tezontepec monogenetic volcanic field, developed between 2.4 and 0.19 Ma ago (Avellán et al., 2019, 2020). In the region of the Acoculco caldera, this volcanic field is manifested by scoria cones and lava flows of basaltic trachyandesite to basaltic andesite composition, interbedded with the products of the caldera complex (Avellán et al., 2020).

Furthermore, the Acoculco caldera is currently defined as a resurgent caldera, and the resurgence has probably been caused by magmatic bodies (i.e. laccoliths, sills and dikes swarms) intruding the Cretaceous limestones at depths >1 km (Avellán et al., 2020).

Despite these recent magmatic ages, no active superficial hydrothermal manifestations have been identified, except for localized emission of cold gases indicative of interaction with the local water table (López-Hernández et al., 2009; Bolós et al., 2022) and Holocene hydrothermal explosions (Canet et al., 2015). However, the possible presence of a geothermal reservoir is indicated by the thermal records obtained by CFE (Comisión Federal de Electricidad, Mexico) in the exploratory wells EAC-1 and EAC-2 drilled in 1994 and 2008, respectively. These wells reached temperatures up to 307.3 °C at 2000 m b.g.l. (Lopez-Hernandez and Castillo-Hernandez, 1997; Gutiérrez-Negrín, 2013). The two boreholes encountered, from the surface: volcanic and volcano-clastic succession, limestone, marble, skarn, granite, and aplitic dyke (bottom hole), this latter dated at 183 ± 36 Ka (Sosa-Ceballos et al., 2018; Avellán et al., 2020).

By this, López-Hernández et al. (2009), Sosa-Ceballos et al. (2018) and Avellán et al. (2020) proposed that the source of the abnormal heat could be a late intrusion of magmatic dykes and sills related to the most recent monogenetic volcanic activity.

Avellán et al. (2019) and Avellán et al. (2020), identified NW- and NE-striking morpho-tectonic lineaments. Such already described lineaments are evident on digital elevation maps (Fig. 4a, b) and appear to correlate, at least to some extent, with the distribution of eruptive centers (Fig. 4c) and hydrothermal alteration (Fig. 4d), even by a qualitative approach. The spatial correlation between eruptive centers,

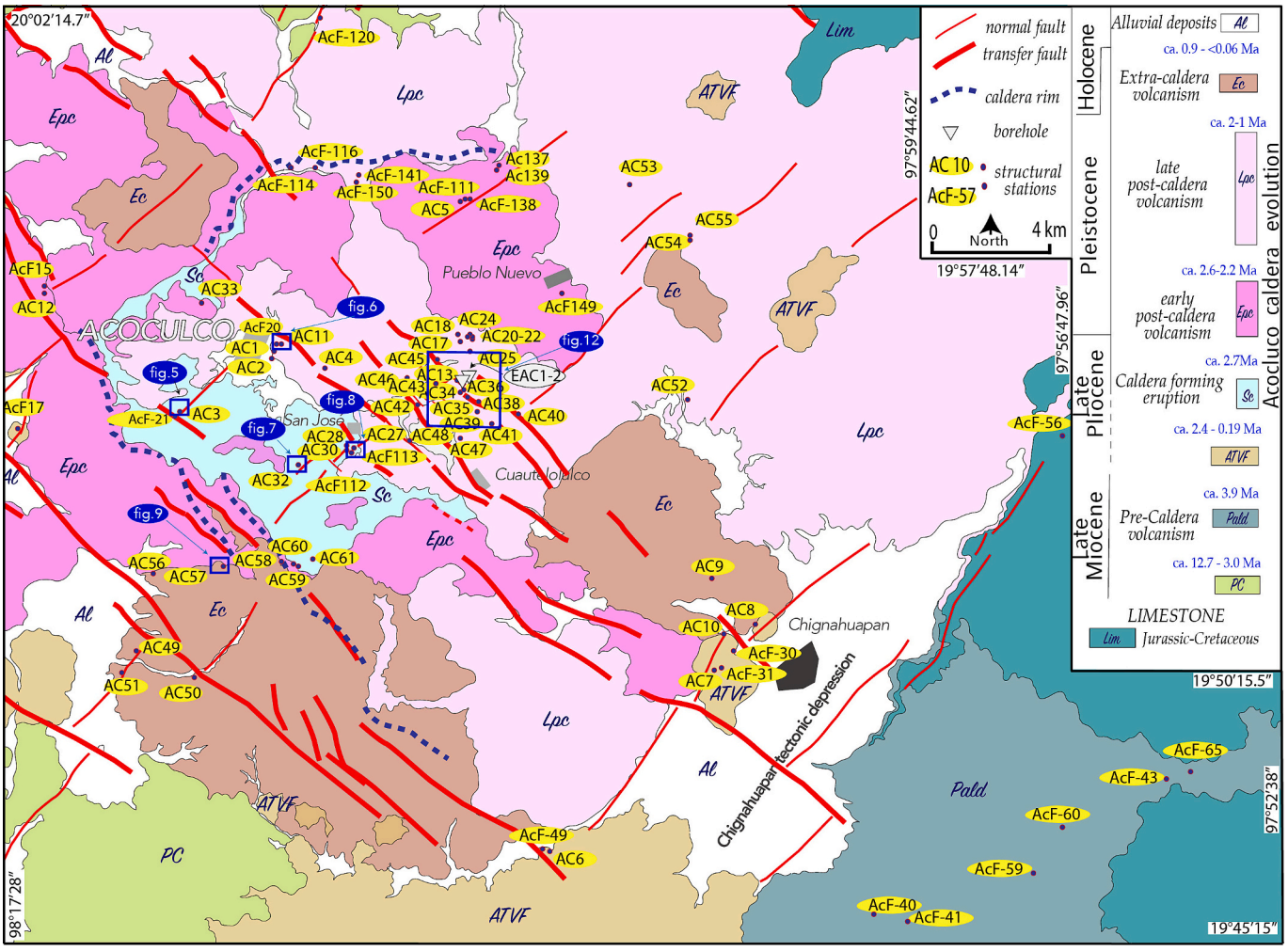

Fig. 3. Geological map of the study area (after Avellán et al., 2019 and Sosa-Ceballos et al., 2018). The blue square corresponds to the area enlarged in Fig. 12. (For interpretation of the references to colour in this figure legend, the reader is referred to the web version of this article.)

hydrothermal alterations and lineaments, provokes the notion that circulation of fluids may be influenced by the regional fault zones, in particular the NW-striking fault system (Gómez-Alvarez et al., 2021).

A complete description of the geological units in the Acoculco area is given in Avellán et al. (2019) and Avellán et al. (2020). For the goals of this paper, we consider eight main units (Avellán et al., 2019; Sosa-Ceballos et al., 2018; Avellán et al., 2019; Avellán et al., 2020), as reported in Fig. 3: six units are related to the volcanic activity encompassed between late Miocene and late Pleistocene; one is related to the Jurassic-Cretaceous carbonate substratum, and the last contains Holocene alluvial deposits.

3. Methods

The data collection of structural and kinematic data is based on observations and measurements on key-outcrops, located along the main structures and where vegetation is scarce, permitting a clear and sufficient large view of the meso-structures. We collected a comparable amount of data in each structural station, to have a general homogeneous data distribution through the study area. Attitude of fault planes and, when possible, kinematic indicators on fault planes (e.g. shear veins, slickenlines, lunate structures, grooves, etc.) were considered to depict the sense of shear. We used the FaultKin (version 8.1.2) and Stereonet (v.3.4.1) free software by R.W. Allmendinger to analyze data on fault kinematics and attitudes, respectively. The geological maps provided by Avellán et al. (2019) and Sosa-Ceballos et al. (2018) constituted the background of our fieldwork.

4. Data analysis

The dataset collected in this study was based on three different inputs, deriving from observations: 1) at map and outcrop scale, to better analyze the geometrical setting of the main fault systems; 2) at outcrop scale, in order to collect, in key outcrops (i.e. structural stations), kinematic data on fault-slip surfaces (see the Appendix: Fig. A1 and Table A1, for data and coordinates of the structural stations); and 3) at detailed map scale (1:10000), in the surrounding of the two dry boreholes. For the sake of simplicity, these different datasets, are described separately in the following sections.

4.1. Two dominant fault systems

Clastic dykes were emplaced into the fractures associated with the NE-striking fault zones. This has been observed at structural stations AC3 (Fig. 5) and AC11 (Fig. 6). In the first case (structural station AC3), a clastic dyke, about 30 cm wide and 60 m long, was injected within fractures parallel to the main normal fault (Fig. 5a) which dissected the volcanic basement and the overlying lacustrine deposits. The clastic dykes crosscut the lacustrine bedding at low angle, display almost sharp contacts and have internal fabric with laminae mostly parallel to the dyke margins (Fig. 5e). Some laminae are formed by matrix supported mm-size (2–3 mm of diameter) clasts (Fig. 5c,d). These latter are

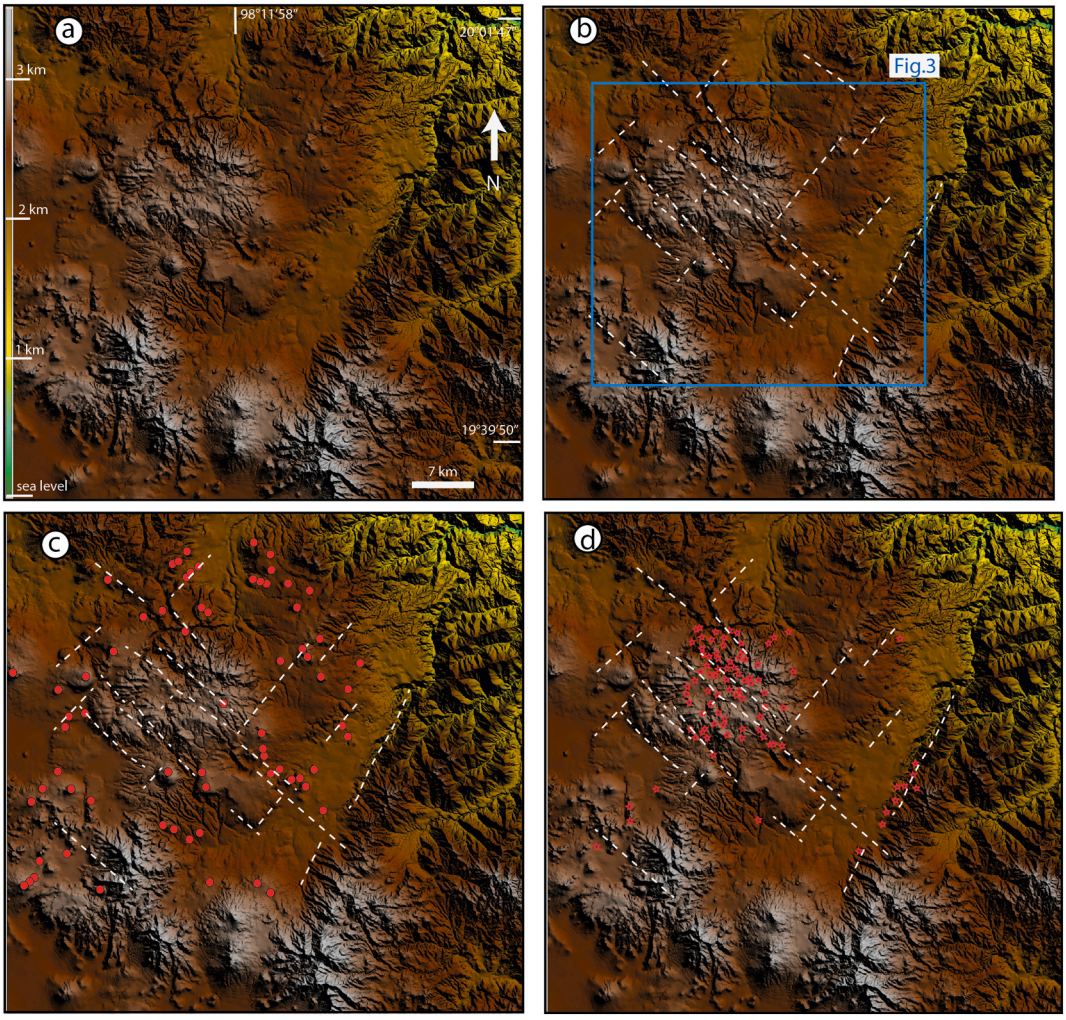

Fig. 4. a) Digital map of the Acoculco study area and surroundings: the colour scale is referred to the altitude; b) main morpho-tectonic lineaments in the area. The square indicates the geological map of Fig. 3. c) relationships between distribution of volcanoes and morpho-tectonic lineaments (after Avellán et al., 2019); d) relationships between distribution hydrothermal mineral ore deposits and morpho-tectonic lineaments (after Román Fernández, 2018).

concentrated in thin (about 5 mm) zones or dispersed within up to 6 cm laminae-thick zones; in this case the size of the clasts is <2 mm. Clasts are mostly formed by the same lithology of the lacustrine deposits and its substratum, made up of pumice, mostly. The age of these injection dykes post-dated the lacustrine deposits (Fig. 3), and are ascribed to the time-range between late Pleistocene and Holocene.

In the second case (structural station AC11), the clastic dykes (up to 40 cm wide) intruded rhyolitic lava flows resting on Holocene lacustrine sediments (Fig. 6). Dykes are intruded into the damage zone of one of the faults belonging to the NW-striking fault system (Fig. 6) and are formed by a massive fabric with clasts (< 2 mm in diameter) made up of sandstone and siltstone of the underlying lacustrine deposits.

Soft-sediment deformation structures (SSDS) at outcrop and map-scale have also been recognized in the AC32 structural station (Fig. 3), where impressive meters- to decameters-scale slumps are exposed (Fig. 7). These latter rest on the hanging wall of a NW dipping normal fault, active during sedimentation. Slumps are mainly formed by highly non-cylindrical folds in which fold axes point to the depocenter.

The NW-striking faults are the most prominent structures in the Acoculco area, for their lateral extension and for the fact that these are mostly intersecting the NE-striking faults. The vertical throw along the NW fault system is estimated to be at least 200 m, on average (Gómez-Alvarez et al., 2021).

The NW-striking fault zones are mostly recognized in the central part of the geological map, bounding the western margin of the Acoculco caldera, and crosscutting the caldera itself. These are dipping to the SW, with an angle between 70° and 80°, in general. Their activity is inferred on the basis of the age of the deformed rocks, and therefore encompassed between late Miocene and Holocene, since some of these dissect the colluvial deposits (Fig. 8), thus indicating their potential, current activity. Noteworthily, these active structures are deforming the same rock volumes previously affected by mineralization and hydrothermal alteration, and by the NE-striking structures (Fig. 8), thus suggesting that deformation is persistent in space and time. As already mentioned, this is also indicated by the distribution of the mineralization and hydrothermal alteration zones, being aligned along the main NW-striking structures (Fig. 2). As an example, Fig. 9 displays one of these main structures, where cataclastic rhyolitic rocks are deeply silicified.

In conclusion, both main NW- and NE-striking faults are active during the same time interval, thus reasonably implying a common stress field, still active.

4.2. *Structural and kinematic analysis*

A total of 445 structural data on faults and fractures were collected in 67 structural stations. During the survey, we recorded the attitude and orientation of the meso-fault slip surfaces and kinematic indicators in structural stations (see Fig. A1 in the Appendix and Fig. 3). These were

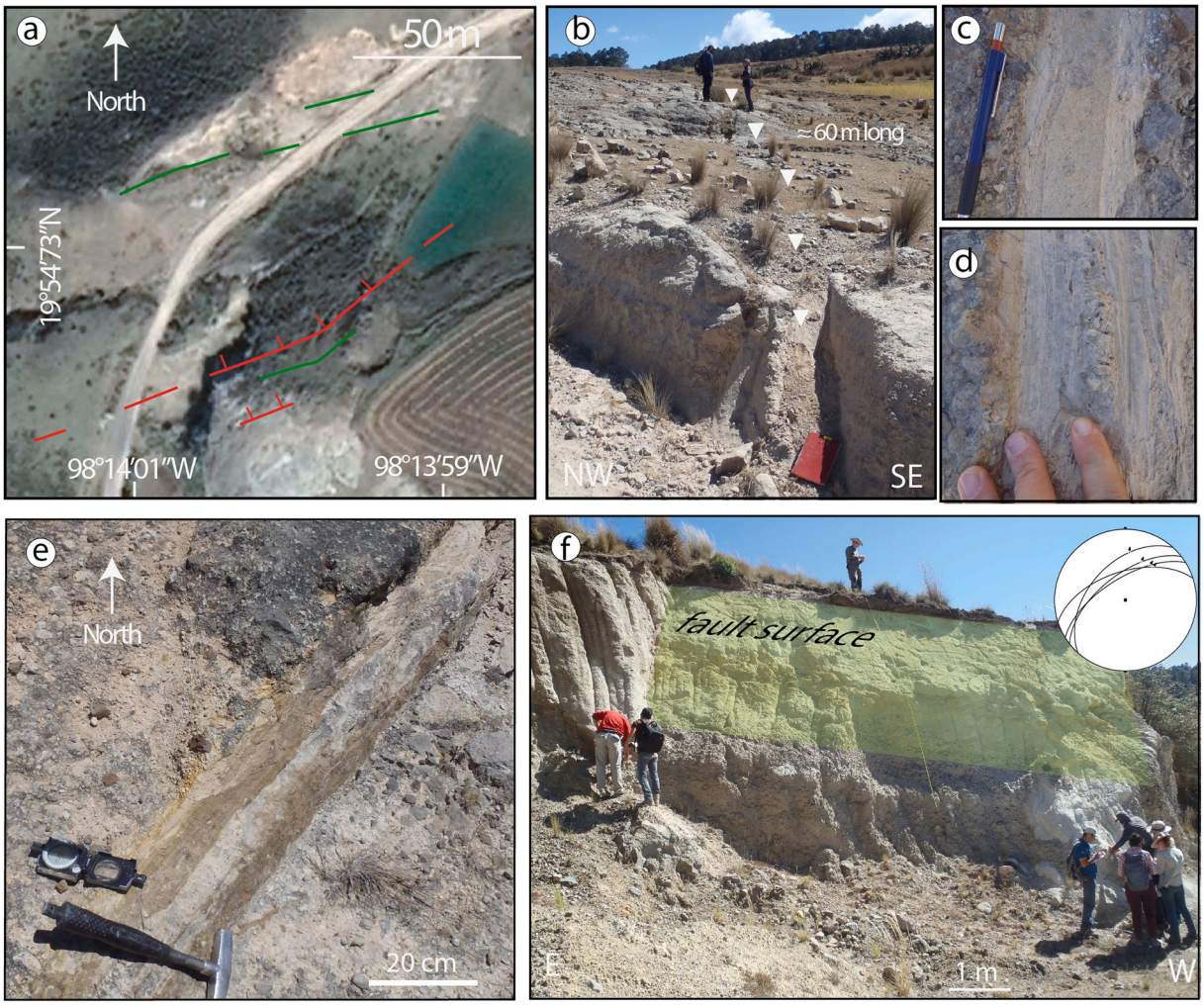

Fig. 5. Relationships between sedimentary dykes and NE-striking normal faults at AC3 structural station. See also Fig. 3 for its location on the geological map. a) Google Earth location map with indication of the sedimentary dykes (green lines) and normal faults (red lines); b) panoramic view of one of the detected sedimentary dykes; c) and d) details of the sedimentary dyke shown in e) concentration of gravels in the central part and lamination structures, due to the injection under fluid-pressure; f) fault surface and related stereonet (lower hemisphere, equal angle projection). (For interpretation of the references to colour in this figure legend, the reader is referred to the web version of this article.)

located mainly along the main fault zones of the fault systems. Kinematic indicators are represented by grooves and mechanical striations, suggesting deformation at shallow structural levels (Fig. 10). Faults cataclasite is composed of fractured rock volumes with comminuted elements, ranging in size from 0.1 to 2 cm. In addition, cataclasite can be locally sealed by silica, hydroxides or carbonates derived from fluids that circulated through the permeable volumes (Fig. 9). A network of joints, overall parallel to the main fault plane is mainly developed in the fault hanging wall, with joints becoming closer spaced (2–4 cm) toward the main slip-surface.

Fault data are reported in the Appendix (Fig. A1), while a synthesis is given in Fig. 11. We recognized dominant and secondary meso-faults characterized by different orientations. The dominant meso-faults are NW- and NE-striking while the secondary meso-faults are N-S and E-W oriented, respectively.

Kinematic indicators on the NW-striking faults can be subdivided in two groups: one indicates movements from left-lateral to right-lateral strike- to oblique-slip (pitches between 0° and 60° and between 120° and 180°, respectively); other points to a dominant normal movement, although with a frequent lateral component (pitch between 60° and 120°). In structural stations where the relationships between kinematic indicators are visible (e.g., AC5, AC6, AC55; Fig. 3) the normal component always overprints the strike-slip to oblique component.

Differently, the NE-striking fault system is consistently characterized by dominantly normal movements, although with a right or left lateral component.

These two main fault systems are then joined to other minor systems, N- and E-striking, respectively. The N-S striking fault system is also characterized by two kinematic indicators, as well as the NW-striking structures. Differently the E-W striking system, is typified by a main normal kinematic movement.

4.3. Borehole surroundings

Because the classification of Acoculco as a hot dry rock system was strongly supported by the drilling results (Lopez-Hernandez and Castillo-Hernandez, 1997; Gutiérrez-Negrín, 2013), we investigated in detail the surroundings of the EAC 1 and EAC2 boreholes. Both boreholes were drilled close to the swampy ground (Los Azufres locality) where emissions of cold CO_2 (Fig. 12) are aligned in the NW direction, parallel to the main structural lineaments, thus suggesting the structural control on the CO_2 emission in agreement with Bolós et al. (2022). Sediments filling the swamp area were affected by soft-sediment deformation structures interpreted as seismites. In addition, the occurrence of sinter deposits, located at their topside (Fig. 12), indicates that the circulation of silica-rich fluids reached the surfacethrough fractures.

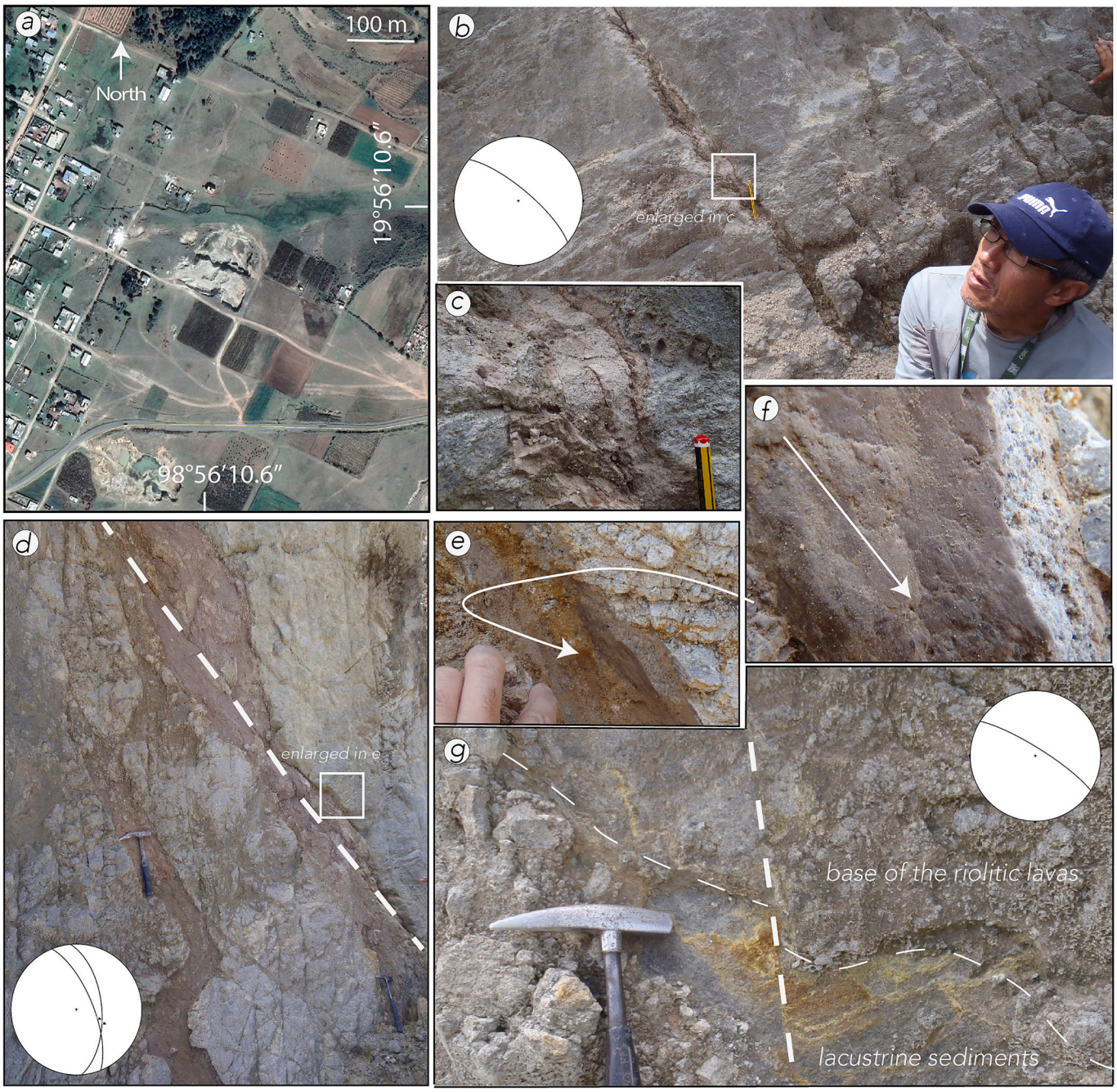

Fig. 6. Relationships between sedimentary dykes and NW-striking fault system at AC11 structural station. See also Fig. 3 for its location on the geological map. a) Google Earth location map. The structural station is centered on the rhyolite dome lava flow; b) sedimentary dyke intruding rhyolite along the NW-SE striking direction; c) detail of the dyke, showing its massive fabric with gravels <0.2 mm in diameter; d) Injected fault zone; d) and e) detail of exposed dyke surface; f) slickenlines recognized on the fault slip surface shown in (d); g) meso-fault affecting the rhyolite substratum, made up of Holocene lacustrine clays. The related stereonets display the attitude of the considered structures (lower hemisphere, equal angle projection).

The collection of structural and kinematic data (Fig. 12) indicates two main sets of faults, NW-SE and SW-NE respectively oriented, and a minor distribution of N-S faults. Fault zones are characterized by fractured rock-volume with joints, almost parallel to the main shear surfaces. Where rock-silicification is diffuse, the cataclasite is characterized by a network of quartz-veins. In other cases, the fault zone can be permeated by sulfate of Fe-hydroxides rich fluids (Fig. 12). Kinematic indicators are always represented by striation on rocks and, less frequently, by mineralized shear veins. In both cases, the normal movement is mostly represented (Fig. 12).

The geological survey highlighted a lacustrine succession to the south of the present swamp (Figs. 12 and 13). Such lacustrine deposit is associated to an older lake, now represented by a 1.5 m thick exposed succession that evolved from about 14,000 to 12,500 cal B.P. (calibrated years before Present), at least. In general, it consists of unconsolidated silt and clay, with embedded, unsorted, sub-rounded clasts, from 5 to 10 cm in diameter. Toward the topside, underneath the Fe-hydroxide silica-sinter deposits concluding the succession and affected by NW-SE striking open fractures, half meter of bedded sediments is observable, with levels of black organic matter (Fig. 14). Significantly, these late Pleistocene lacustrine sediments are deformed by seismites (i.e., soft-sediment deformation structures, developed during seismic events, $M \geq 5$) that affected decimeter-thick levels. Seismites consist of faults, slumps, injection dykes made up of fluidized sediments and/or silica-rich fluids.

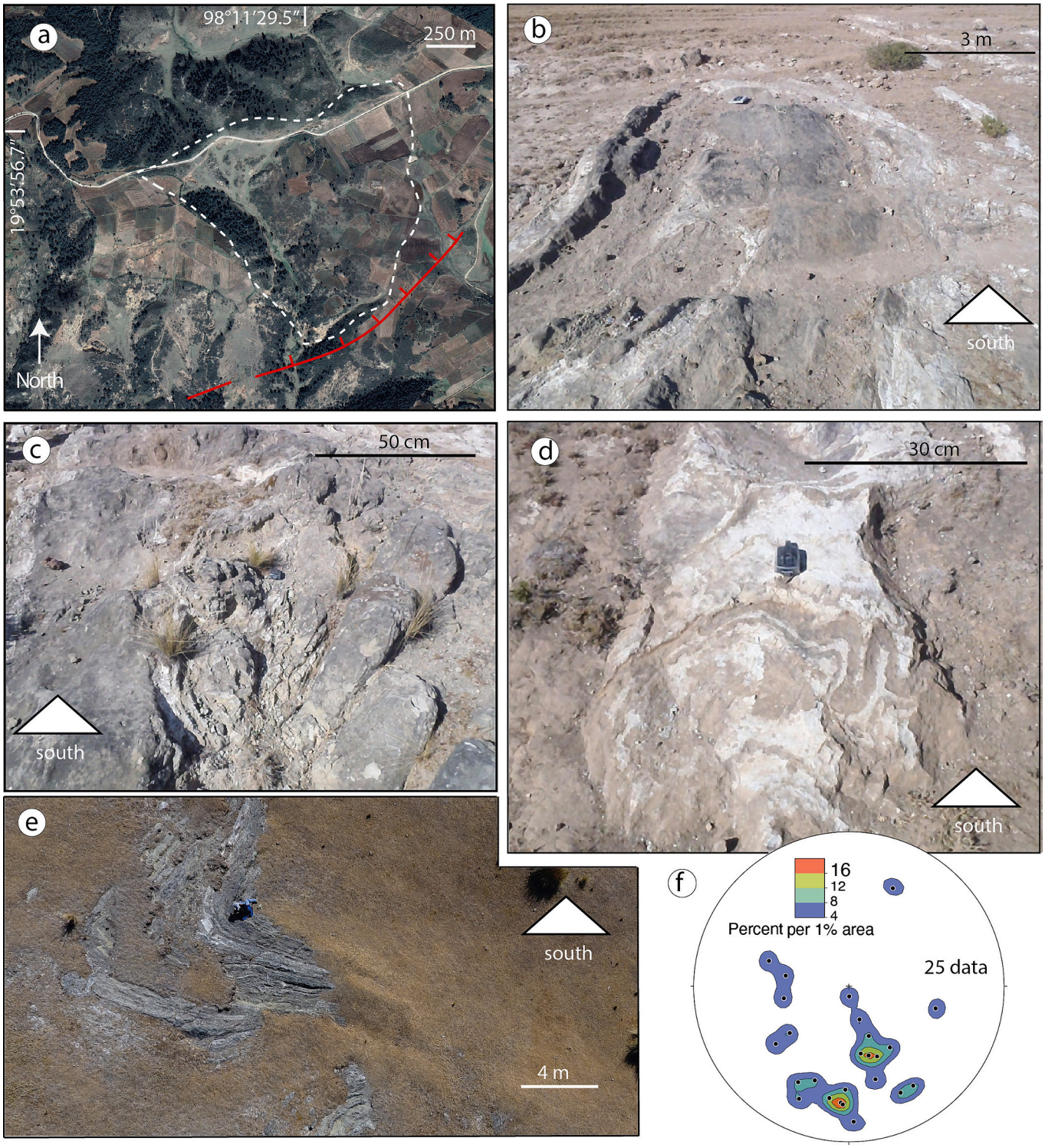

Fig. 7. a) Google Earth location map indicating the area (AC32 structural station; see also Fig. 3 for its location on the geological map) where lacustrine sediments affected by slumps are cropping out (white dashed line); the normal fault delimiting this basin is also reported (red line); from b) to e): examples of highly non cylindrical folds at different scale of observation; f) diagram (lower hemisphere, equal area) indicating the distribution of the hinge lines. (For interpretation of the references to colour in this figure legend, the reader is referred to the web version of this article.)

The age of the sediments (time-interval between 12,871 and 12,900 cal B.P., Fig. 13) can be considered as the age of the seismic event.

X-ray powder diffraction analysis of lacustrine samples shows an enrichment from Kaolinite to Buddingtonite (Fig. 13), accordingly to what has been previously observed in the Acoculco surroundings (Quinto et al., 1995; Canet et al., 2010). This evidence may indicate alteration of feldspar in an acid environment, progressively passing to ammonium-rich waters, hence suggesting that geothermal fluids were mixed with the fresh waters of the lake, and that hydrothermal fluids are active in the area since ca. 12,000 years, at least.

The occurrence of diatoms provides us information on the water column. At the base of the sedimentary succession, in the bedded clays,

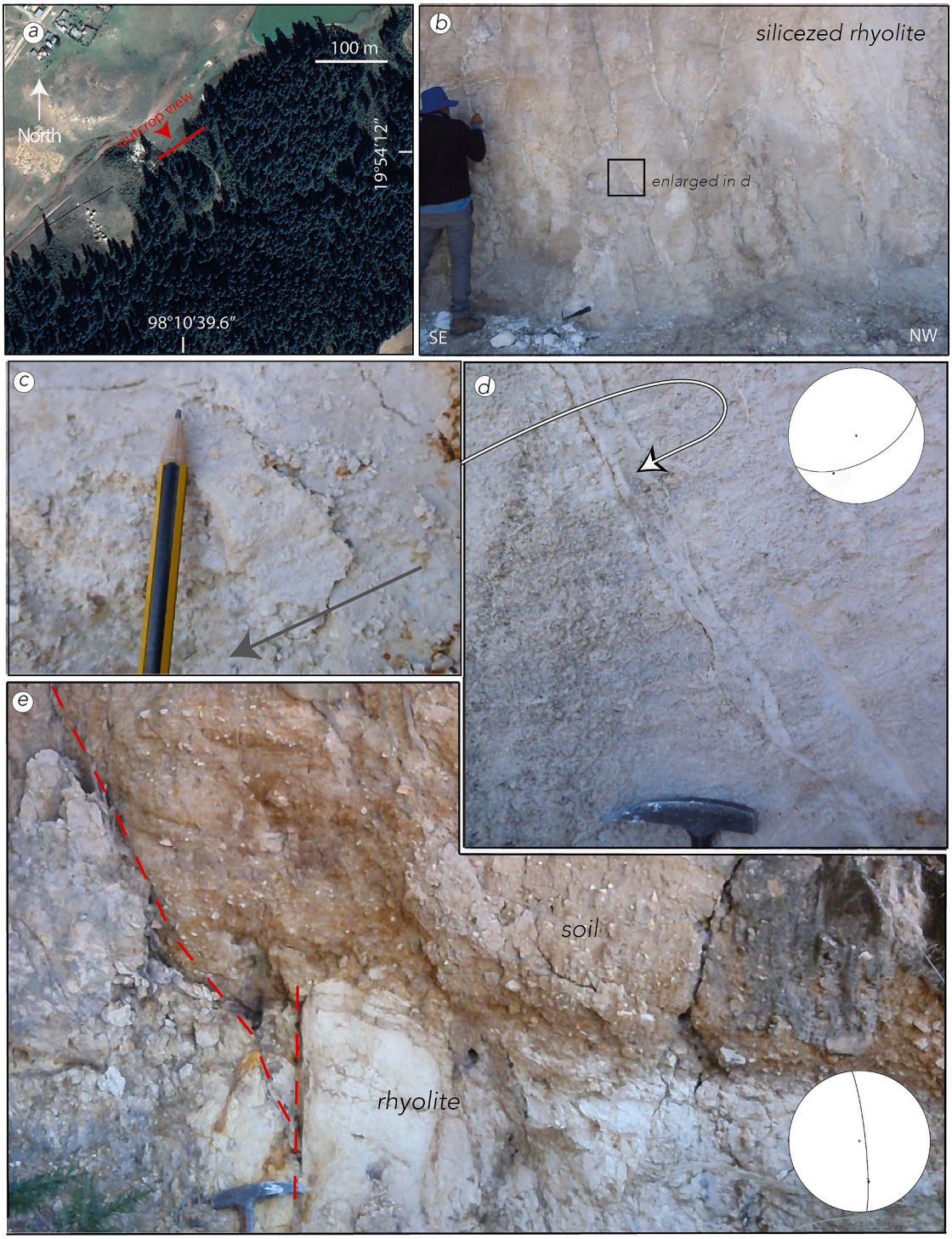

Fig. 8. a) Google Earth location map indicating the outcrop location (structural station AC30). See also Fig. 3. The photo-view is also indicated; b) fractured and silicified rhyolite in the damage zone of the NE-striking fault zone; c) and d) details of the fault and kinematic indicators on the fault surface, respectively; e) NW-oriented fault cross-cutting the rhyolite and soil.

the diatomite Eunothia sp. dominates, suggesting a clayey-rich shallow environment. Subsequently, the habitat drastically changes toward a relatively deeper water column, as indicated by the presence of Pinnularia sp. Regarding the age of this variation, this is encompassed between the warm Bølling-Allerød and cold Younger Dryas (Dansgaard et al., 1993; Andersen et al., 2004) time-intervals, occurred in the final stages of the last glacial period.

5. Discussion

Assuming that the measured slickenlines are parallel to the main shear stress, then kinematic and geometrical data from fault surfaces can be used to get paleo-stress analysis (Angelier, 1979). This analysis is graphically represented by the double-couple fault-plane solution diagrams (Fig. 15) we analyzed for the different systems of meso-faults (Fig. 11).

As previously indicated, the NW-striking faults are characterized by

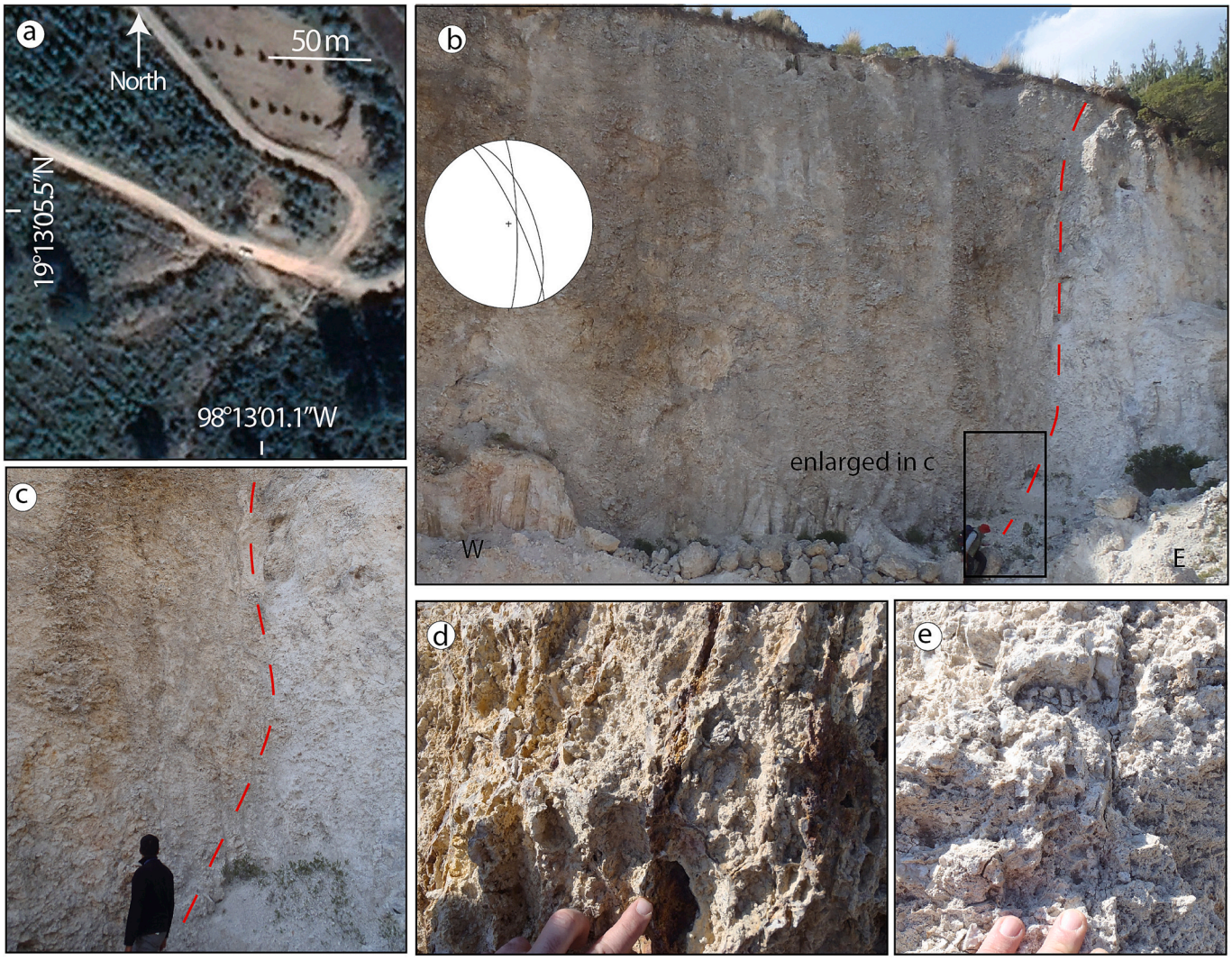

Fig. 9. Hydrothermal alteration along a NW-SE oriented fault zone (structural station AC57); a) Google Earth location map centered on the outcrop location; see also Fig. 3. b) The width of the altered rock-volume is of about 25 m; the dashed red line indicates the main slip-fault surface of which attitude is reported in the stereonet (lower hemisphere, equal angle projection); c) detail of the core fault zone; d) and e) examples of veining in the damaged rock, testifying the role of fractures in channeling hydrothermal fluids. (For interpretation of the references to colour in this figure legend, the reader is referred to the web version of this article.)

two movements on their slip-surfaces, the older of which is defined by a strike-slip to oblique right-lateral movement. The paleo-stress analysis of this event indicates that the minor kinematic axis (assumed parallel to the minor stress axis) is NW-striking, similarly to the orientation shown by the paleo-stress analysis on the NE-striking normal faults (Fig. 15). This implies that normal faults and strike-slip to right-lateral oblique-slip faults are kinematically compatible, although these are almost perpendicular each other. This structural condition can be explained assuming that the NW-striking faults played the role of transfer zones, thus acting contemporaneously with the NE-striking normal faults, in the frame of the regional extensional tectonics characterized by the NW-stretching direction, active since middle Miocene (García-Palomo et al., 2018; Sosa-Ceballos et al., 2018; Avellán et al., 2020; Olvera-García et al., 2020). In this framework, injection of unconsolidated sediments into fractures (structure, structural stations AC3 and AC11, Figs. 5 and 6) is a consequence of deformation (i.e., paleo-seismicity) assisted by fluid pressure (Palladino et al., 2018, 2020; Alsop et al., 2022 with references), determining laminar to turbulent flow when fluid pressure balances or overtakes the grains weight, respectively (Knipe, 1986). It implies that the described clastic dykes are co-seismic effects, indicating tectonic activity most likely occurred during the latest Quaternary. In this view, another clear example of paleo-seismicity is displayed by the *syn*-sedimentary folds (slumps, structural station AC32, Fig. 7) developed during a *syn*-sedimentary gravitational process involving unconsolidated sediments, triggered by seismic-induced shacking (Alsop and Marco, 2011; Waldron and Gagnon, 2011). The age of these lacustrine sediments is unknown. However, considering the age of the volcanic basement (Fig. 3), the lacustrine sediments affected by the soft-sediment deformation, could be younger than late Pliocene.

As regards the relation between geological structures and fluid flow, the kinematic characteristics of transfer zones are surely favorable for maintaining pathways along which hydrothermal fluids and magmas, can be easily channeled (cfr. Dini et al., 2008; Liotta et al., 2015; Liotta and Brogi, 2020). This is a consequence of the intermediate axis orientation that, being close to the vertical, favors the ascent of deep fluids (Sibson, 2000; Rowland and Sibson, 2004). Noteworthily, the distribution of hydrothermal manifestations and volcanoes agree and follow the NW-trends, mainly (Fig. 2).

The second kinematic event recorded on the NW-striking fault-surfaces is dominantly normal. Conversely, two distinct kinematic events were not recognized on the NE-striking fault system. From this we infer that kinematics did not significantly change for the NE-striking structures, from the first to the second deformational event. Therefore, we propose that the temporal change in the kinematics of the NW-striking

Fig. 10. From strike-slip to normal slip examples of kinematic indicators characterizing the faults in the study. In a few cases, Fe-hydroxides shear veins can also be found on fault-slip surfaces.

faults was consequent on the onset of magmatic uplift. The competition between extension and uplift determines the role of the NW-striking faults, initially developed as transfer faults when extension is dominant, and, subsequently, reactivated as normal faults when uplift controlled the evolution. This also accounts for the maintenance of kinematics in the NE-striking structures.

In this framework, the N-S and E-W striking secondary meso-faults, are interpreted as minor structures associated to the NW- and SW-striking regional faults (Fig. 15), respectively. Furthermore, their related kinematic indicators are compatible with those recognized on the slip-surfaces of the regional faults to which are joined.

The novelty of this interpretation is that it considers the observed deformation in a common extensional framework, without envisaging variation of the regional stress field during the Miocene-Pleistocene time, as it was concluded by previous authors (e.g., García-Palomo et al., 2002a, 2002b; García-Palomo et al., 2018).

Several authors (e.g., Peacock and Sanderson, 1991; Kim et al., 2004; Fossen and Rotevatn, 2016) described the structural interaction among faults, and their role in significantly increasing the permeability (e.g. Curewitz and Karson, 1997; Micklethwaite et al., 2015) in fault step-over zones (e.g., Kim et al., 2004; Faulds et al., 2011; Micklethwaite et al., 2015; Brogi et al., 2021) and/or in localized sectors of

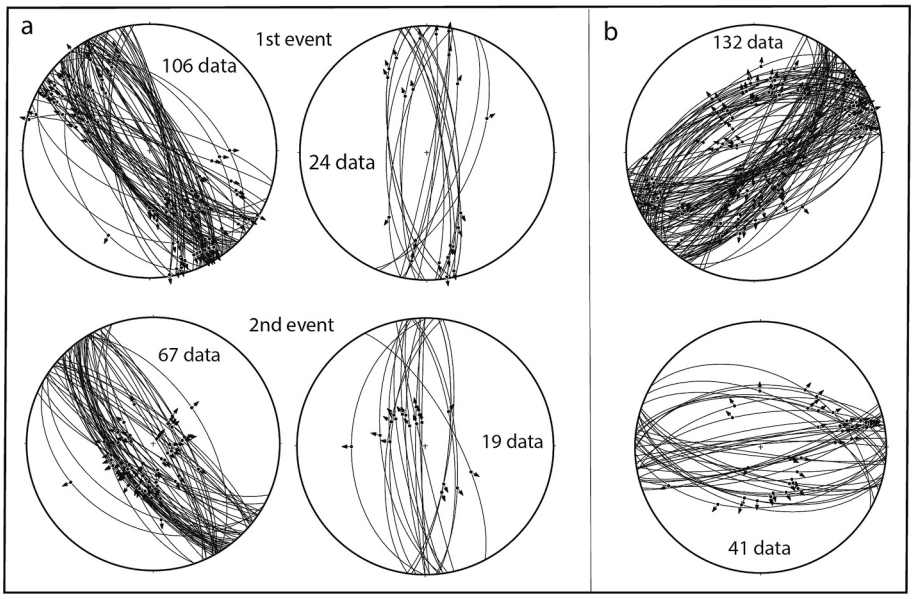

Fig. 11. Compilation stereonets (lower hemisphere, equal area projection) of the collected kinematic data, subdivided by orientation and number of recognized kinematic events. a) NW-striking and N-striking faults displayed two kinematic indicators of which crosscutting relationships (see also Fig. 10) permitted to divide the kinematic evolution in two events; b) in contrast, the SW-striking and E-striking faults displayed one group of kinematic indicators.

transtensional fault zones where magmatic (Pérez-Flores et al., 2016; Mathieu et al., 2011) and/or hydrothermal fluids (Faulds et al., 2011; Micklethwaite et al., 2015; Liotta et al., 2015; Brogi et al., 2021) can be localized. In this view, the location of the Acoculco caldera accounts for being strictly connected to the permeability induced by the fault geometry and kinematics: assuming that the collapse affected the full extent of the magma chamber, we infer that the NW-striking fault delimiting the western side of the caldera at surface (Fig. 3), likely delimited the magma chamber at depth, thus determining an asymmetric collapse.

In this view, the role of pre-existing structures controlling caldera locations was investigated by Maestrelli et al. (2021), concluding that inherited discontinuities may affect caldera collapse by inducing rectilinear caldera faults that generate non-circular ring faults. This is comparable with the western border of the Acoculco caldera and other similar contexts such as, among many others (e.g. Acocella and Funiciello, 1999; Milner et al., 2002; Petrinovic et al., 2010) those described by Ferguson et al. (1994) in Nevada, where NNE-striking faults controlled the collapse of the Silent Canyon caldera; or, by Acocella et al. (2002) in the Ethiopian Rift, where caldera locations and their evolution is linked to pre-existing rifting structures.

In particular, the occurrence of pre-existing vertical structures, such as transfer faults, requires the smallest magmatic pressures to be penetrated (Acocella et al., 1999), reasonably favored by the kinematics of the transfer zones (i.e., the attitude of the intermediate stress axis). In this context, Pérez-Orozco et al. (2021) described the evolution of the Acoculco magmatic system, through different tectonic pulses that promoted the ascent and mixing of magmas that triggered the eruption and the caldera collapse.

In exposures surrounding the exploration boreholes, faults are characterized by hydrothermal mineralization coeval with their vertical movement. This accounts for considering fault permeability reasonably reduced by sealing processes, as already suggested by previous authors (López-Hernández et al., 2009; Viggiano-Guerra et al., 2011; Lorenzo-Pulido et al., 2011; Peiffer et al., 2014; Canet et al., 2015; Bolós et al., 2022).

However, sealing of fractures is in competition with tectonic activity and seismicity; field evidence suggests that the Acoculco area is a tectonically active area, as indicated by late Pleistocene-Holocene seismites (Fig. 13), dyke injections in NE-striking fault zones (Figs. 5 and 6), NW-striking faults cross-cutting the colluvium (Fig. 8), and recent gas and fluid-escape and blowouts (e.g., Canet et al., 2015). Then, the fact that CO_2 bubbling in the swamp area is aligned to the main NW-striking fracture zone (Fig. 12) indicates that the hydraulic conductivity is still controlled by deformation through which only gas can pass through the very recent clays (Bolós et al., 2022).

Concluding, fracture sealing appears as the most efficient process, despite from the evidence of recent seismicity observed in the surrounding of the Acoculco caldera (Esquivel-Mendiola et al., 2022; Perton et al., 2022).

An explanation of this derives from the study of the lacustrine deposits in the area adjacent to the boreholes (Fig. 12a). The results clearly indicate a northwards migration of sedimentation, which also implies a coeval migration of deformation.

Applying this information at regional scale, this shed light on reasons why permeability results scarce or absent in the borehole area whereas it could be reasonably present northwards.

Another factor negatively influencing permeability is the fluidization of sands. As described, it can occur in the damage zone of the fault zones when these insist onto an over-pressured units (Palladino et al., 2018). Injection dykes intruding fault zones can in fact act as a hydraulic barrier, filling up voids and fractures and obstructing hydrothermal fluid flow.

Hence, the NW-striking transfer faults appear to be the most suitable for channeling deep fluids, given their kinematics and the orientation of their intermediate axis (Fig. 2), switching from almost vertical to almost horizontal during their kinematic evolution from dominantly strike-slip to normal slip movements.

6. Conclusions

Eruptive center locations, caldera collapse and circulation of hydrothermal fluids are controlled by the interplay between transfer and normal faults, in the frame of the regional NW-striking extension, competing with the uplift induced by the partial melting of the lithosphere, determining anomalous heat flux (Fig. 16). When crustal stretching is dominant, deep fluids can be addressed in localized almost vertical structural channels, along the NW-striking faults, since the

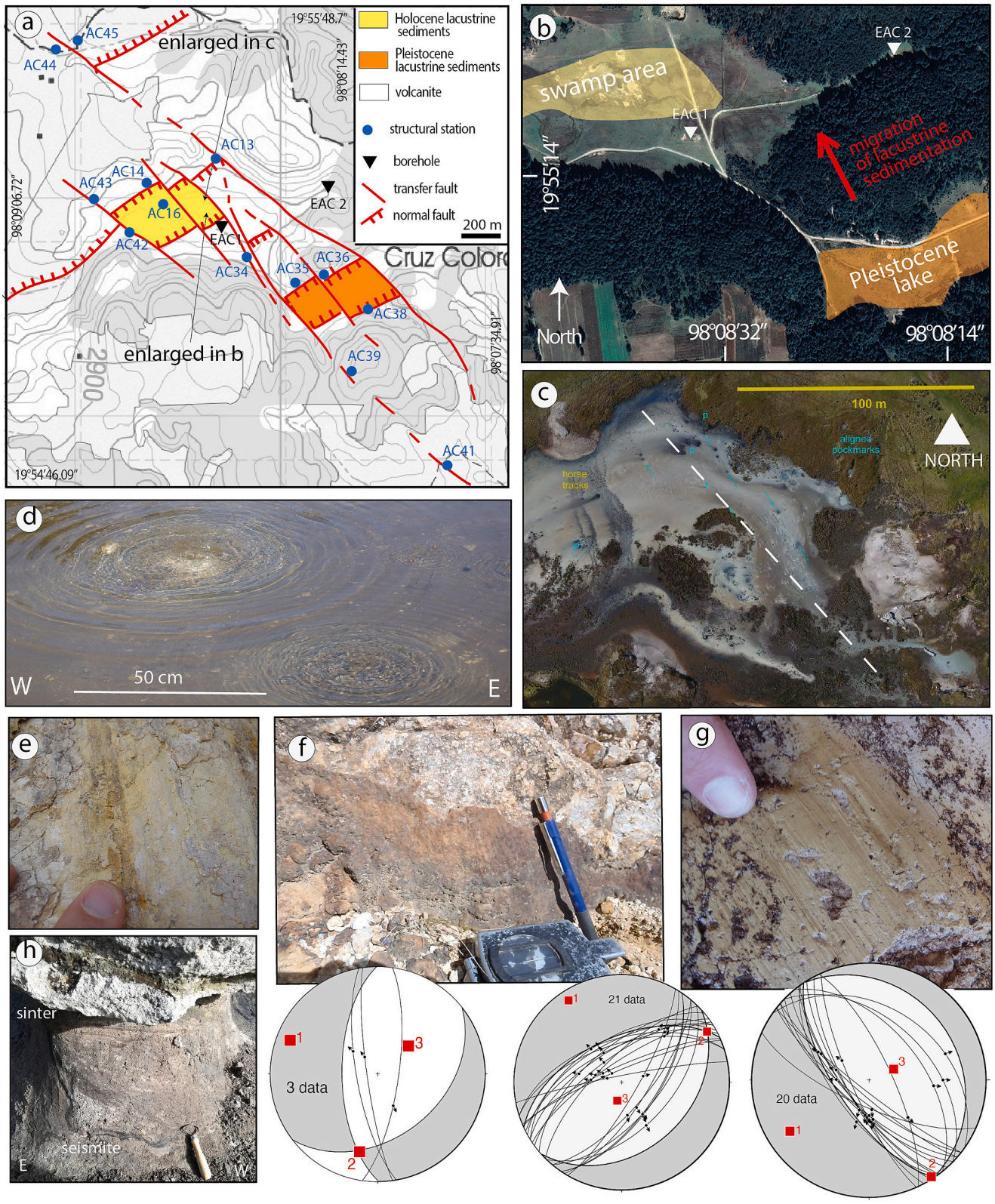

Fig. 12. Survey in the surroundings of EAC1 and EAC2 boreholes. See also Fig. 3. a) structural map showing the main features and the location of the structural stations of which stereonets are reported in the Appendix (Fig.A1); b) Google Earth image of the study area: the past and present lacustrine environments are indicated, highlighting the migration of the lacustrine environment northwestwards; c) aerial photo of the swamp area: the dashed line indicates the alignment of CO2 bubbling, consistent with the main NW-striking fault system; d) example of bubbling in the swamp area; e-f-g) examples of Fe-hydroxides and sulfate shear veins on fault slip surfaces, indicating the sealing process affecting fractures; h) lacustrine sediments are affected by seismites, indicating tectonic activity during Holocene; the lacustrine sedimentation is then concluded with a cap of silica-sinter deposit. Cumulative stereonets (lower hemisphere, equal angle projection) illustrating fault surface attitudes, related kinematic indicators and their inversion to focal mechanisms, to depict the orientation of the main stress axes (1 > 2 > 3), assuming slickenlines parallel to the main shear stress.

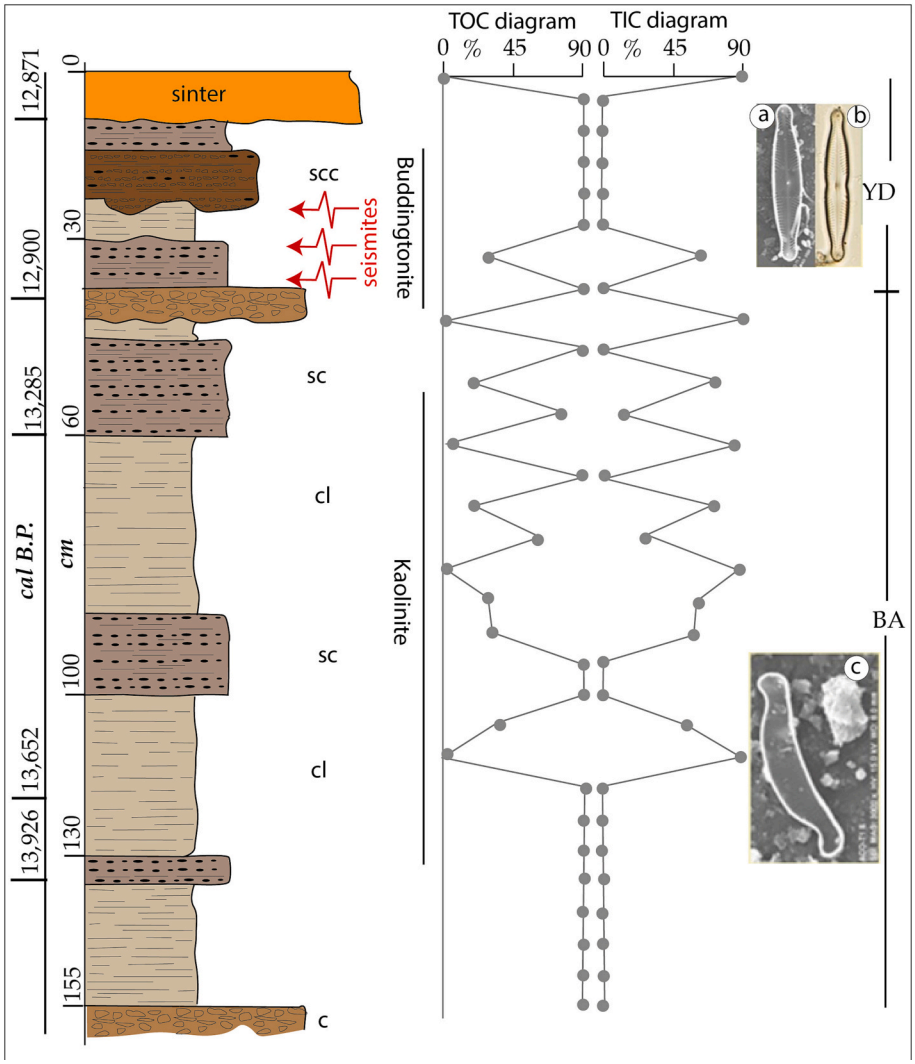

Fig. 13. Right: Stratigraphic column of the exposed succession, as reconstructed from ground level. Ages are given in calibrated years before Present (cal B.P.). Seismites location is indicated by the red arrows and are encompassed between 12,800 and 12,700 cal BP. Occurrence of Kaolinite and Buddingtonite (hydrothermal minerals deriving from alteration of feldspars), in the sediments, at the related intervals, suggests coeval presence of geothermal fluids in the lake. Left: The cyclicity observed in the Total Organic Carbon (TOC) and its specular Total Inorganic Carbon (TIC) diagrams are indication of the cyclicity of the humid phases. The diatom Eunothia sp. (c) suggests acid environment while a saline water is indicated by the diatoms *Pinnularia interrupta* (a) and Pinnularia amabilis (b). Bølling-Allerød and Younger Dryas periods are indicated as BA and YD, respectively. Symbols: c- conglomerate; cl- clay; sc - silty clay; scc – silty clay with levels of conglomerates. (For interpretation of the references to colour in this figure legend, the reader is referred to the web version of this article.)

intermediate stress axis is close to vertical.

Conversely, when uplift is dominant, pre-existing structures, independently by their orientation, are affected by normal and dilatational movements, favoring lateral migration of the fluid flow (the intermediate axis is close to horizontal), through structures hydraulically connected with the transfer zones, i.e., at the intersections between normal and transfer faults and/or stepover zones.

Permeability is therefore controlled by the evolution of deformation, in competition with sealing processes, both determined by injection of clastic dykes and hydrothermal minerals formation.

Hence, in this extensional context, we can envisage that deep fluids are mainly channeled along the NW-striking structures and then laterally migrated when the NW-striking fractures are hydraulically connected to the NE-striking normal faults.

Lastly, the lack of permeability in the borehole area accounts for sealing of fractures after hydrothermal minerals deposition. Considering the age of the sediments affected by the seismites, the loss of permeability appears to be a very recent event, although diffuse.

Finally, indications from the lacustrine sedimentary evolution in the borehole surroundings suggest that a northward migration of deformation is acting, reasonably accompanied by permeability, that would be therefore more favorable along the NW-striking structures, and to the North of the present Acoculco caldera collapse location. Our results recognize: (a) the NW-striking structures as those with the most recent activity and where the favorable permeability conditions can develop; (b) the migration of deformation northwestwards through time, explaines the scarce permeability of the explored area by drillings; (c) the fault behavior appears to switch in response to periods of increased partial melting of the lithosphere, and this influences fluid pathways, in turn controlled by the tectonic segmentation.

Author agreement statement

We the undersigned declare that this manuscript is original, has not been published before and is not currently being considered for publication elsewhere.

We confirm that the manuscript has been read and approved by all named authors and that there are no other persons who satisfied the

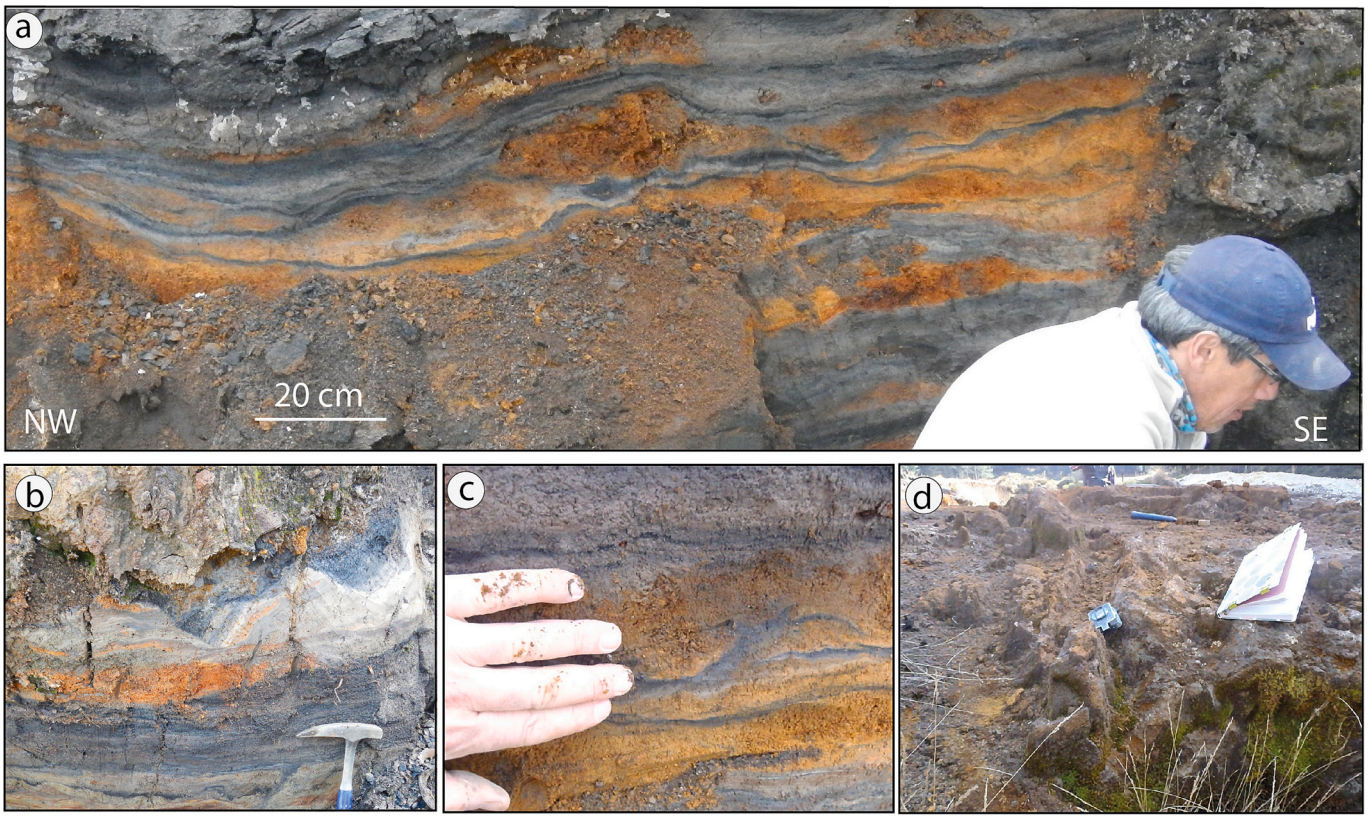

Fig. 14. Seismites in the Pleistocene lacustrine environments: a) deformed beds composed of silt and organic matter; b) and c) details of the soft-sedimentary structures; d) hydroxide-silica sinter deposit at the top of the lacustrine succession: the NW-striking fracture from which the saline fluids raised up is visible.

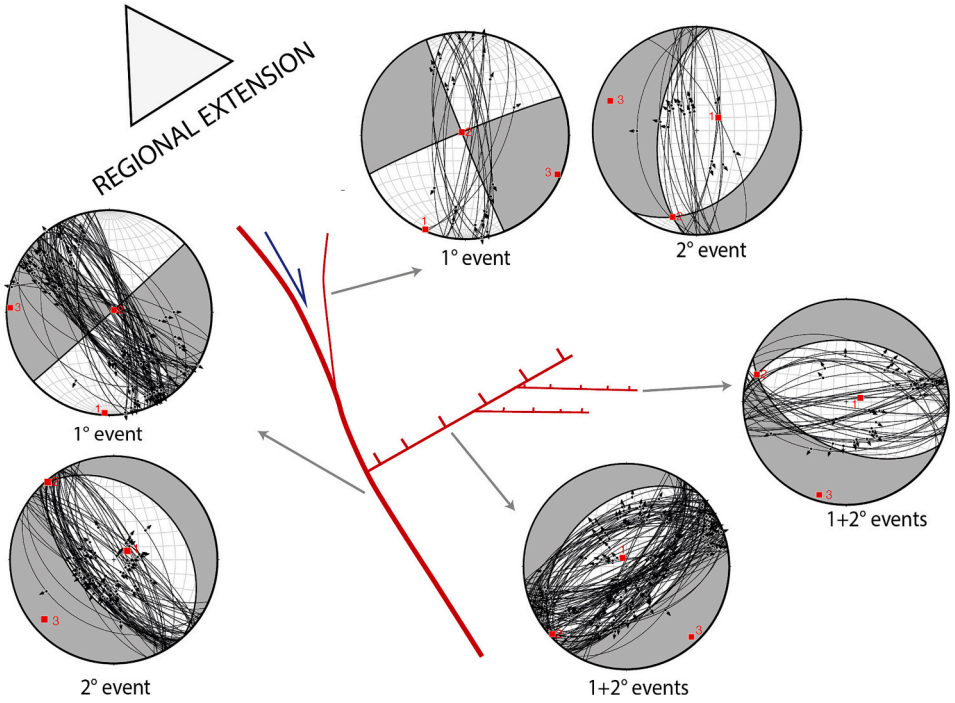

Fig. 15-. Focal mechanisms from inversion of kinematic data (see also Fig. 11) and their interpretation in the frame of the NW-striking regional extension characterizing this sector of the Trans Mexican Volcanic Belt. Kinematic axes, assumed parallel to stress axes, are indicated as $1 > 2 > 3$.

criteria for authorship but are not listed. We further confirm that the order of authors listed in the manuscript has been approved by all of us.

We understand that the Corresponding Author is the sole contact for the Editorial process. He/she is responsible for communicating with the other authors about progress, submissions of revisions and final approval of proofs.

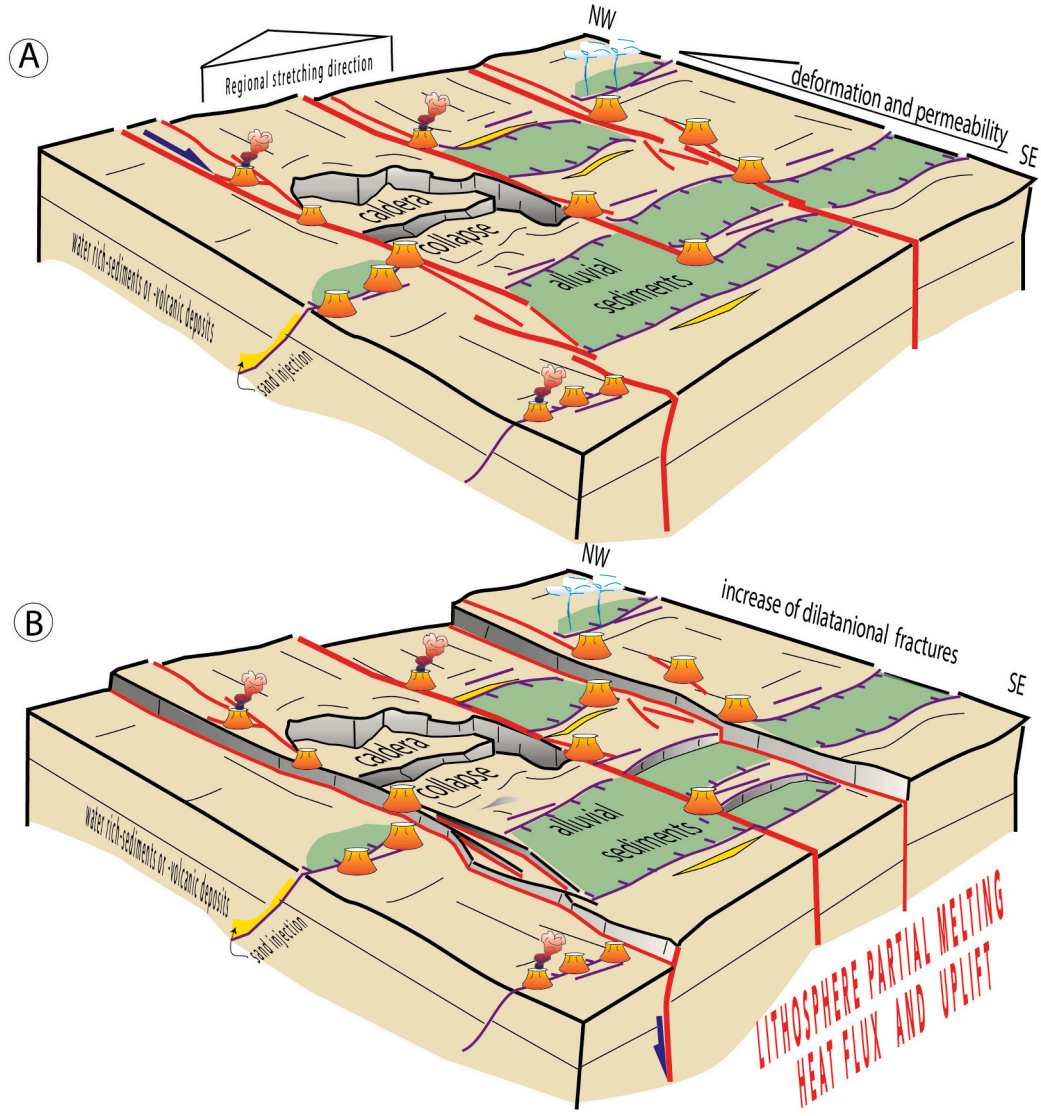

Fig. 16. Conceptual models illustrating the interplay between crustal stretching and uplift induced by lithosphere partial melting. A) : when stretching is dominant, the NW-striking structures play the role of transfer zone and the SW-striking normal faults accommodate extension. Fluids are channeled following the attitude of the intermediate axis that, being almost vertical along the NW-structures, can favor the up-flow of deep fluids, laterally migrating along the normal faults; B) when uplift is dominant, as induced by lithosphere partial melting and subsequent heat flux, the pre-existing structures are re-activated as normal faults independently by their orientation. The interplay between stretching, magmatism and fault linkage geometries, contributed to determine the condition for the Acoculco caldera collapse.

Declaration of Competing Interest

Domenico Liotta reports a relationship with Horizon 2020 European Innovation Council Fast Track to Innovation that includes: funding grants. José Luis Macias, JVGR co-editor and co-author of this manuscript.

Data availability

Data will be made available on request.

Acknowledgments

This manuscript is dedicated to the memory of Victor Hugo Garduño-Monroy, prematurely passed away. Victor Hugo actively participated to the collection of data and to the preliminary analysis of the data. We are confident to have correctly interpreted our unforgettable friend's thoughts. Victor Roche suggestions helped us to improve our manuscript. This work was supported by European Union's EU Horizon 2020, Grant Number 727550 (GeMex project), and by the Mexican government, Grant Number 268074. We are grateful to two anonymous Reviewers and to the Editor, Shane Cronin, for their constructive comments and inputs.

Appendix A

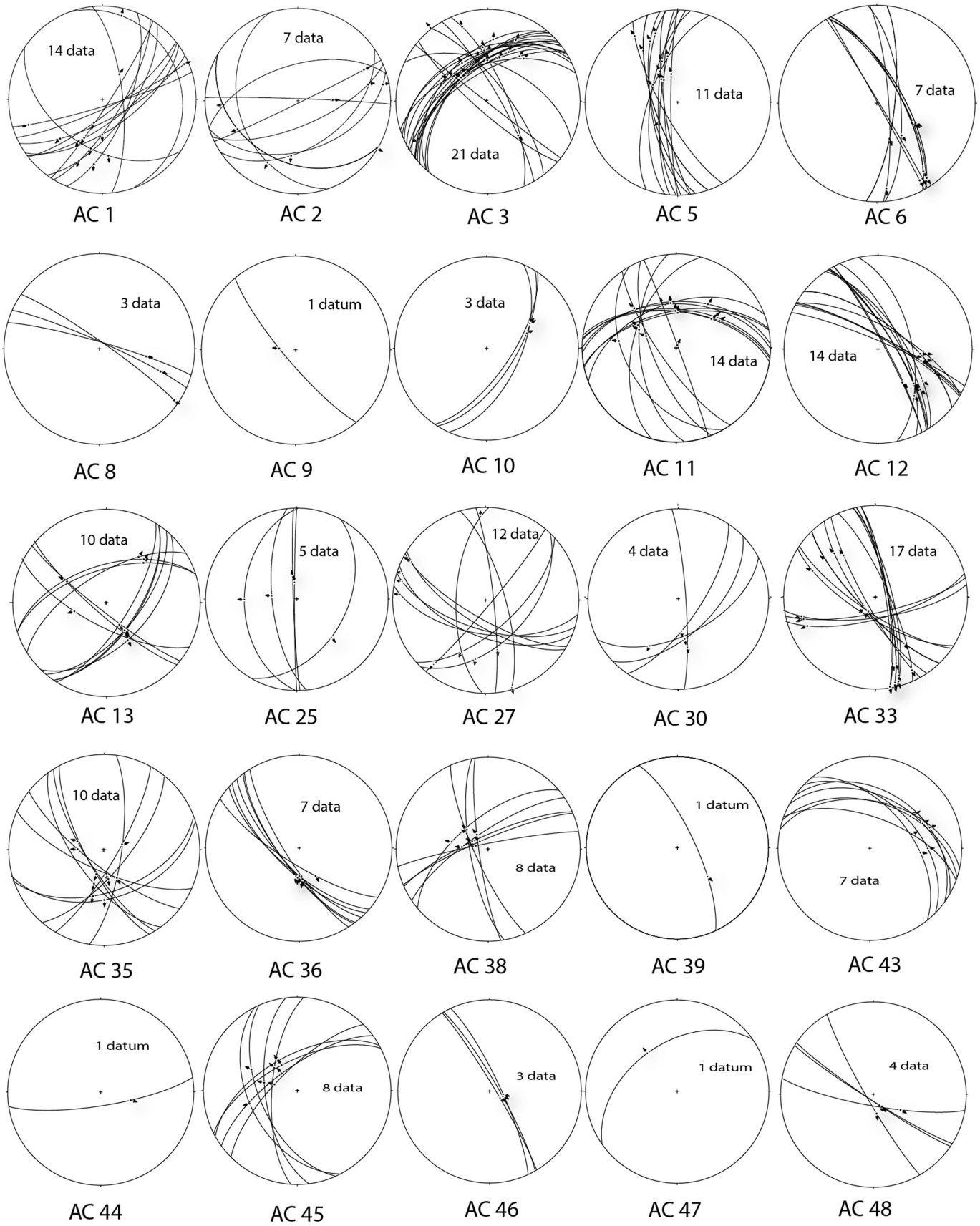

Fig. A1. Stereonets (lower hemisphere, equal angle projection) related to the structural stations reported in Fig. 3. See also Table A1 for location. Number of data and name of the station are indicated for each diagram.

Table A1
UTM coordinates (Zone 14Q) related to the structural stations shown in Fig. 3.

Structural station	x	y	Structural station	x	y	Structural station	x	y	Structural station	x	y
Struct. stations with kinematic indicators			AC38	590,338	2,202,700	ACF30	598,990	2,194,425	*Struct. stations without kin. Indicators*		
AC1	583,352	2,204,246	AC39	590,285	2,202,378	ACF31	598,431	2,193,582	AC3	580,201	2,202,239
AC2	583,196	2,204,005	AC43	589,067	2,203,162	ACF40	603,708	2,185,359	AC35	590,000	2,202,786
AC3	580,201	2,202,239	AC44	588,909	2,203,848	ACF41	604,781	2,185,196	AC38	590,338	2,202,700
AC5	589,453	2,209,342	AC45	589,001	2,203,884	ACF49	592,843	2,187,537	AC39	590,285	2,202,378
AC6	592,842	2,187,539	AC46	587,868	2,203,430	ACF56	609,806	2,201,401	AC40	591,561	2,202,263
AC8	599,757	2,195,136	AC47	589,697	2,201,424	ACF59	609,272	2,187,113	AC41	590,739	2,201,945
AC9	598,381	2,196,801	AC48	587,957	2,201,330	ACF60	610,317	2,188,531	AC42	589,244	2,203,041
AC10	598,807	2,194,882	AC50	580,697	2,193,239	ACF65	614,525	2,190,455	AC43	589,067	2,203,162
AC11	583,470	2,204,514	AC52	597,339	2,202,790	ACF111	589,481	2,209,342	AC46	587,868	2,203,430
AC12	575,479	2,206,331	AC53	595,291	2,210,051	ACF112	586,084	2,201,082	AC47	589,697	2,201,424
AC13	589,665	2,203,339	AC54	593,246	2,214,129	ACF113	585,902	2,201,035	AC51	578,500	2,193,311
AC25	589,938	2,204,456	AC55	593,225	2,214,261	ACF114	584,093	2,210,387	AC53	595,291	2,210,051
AC27	586,092	2,201,057	ACF15	575,726	2,206,457	ACF120	584,790	2,216,096	AC57	581,794	2,196,963
AC30	585,903	2,201,033	ACF17	574,688	2,201,435	ACF137	590,962	2,210,318	AC58	583,768	2,197,177
AC33	580,847	2,205,934	ACF20	583,487	2,204,496	ACF138	589,813	2,209,535	AC60	584,212	2,197,077
AC35	590,000	2,202,786	ACF21	580,199	2,202,245	ACF139	589,679	2,209,468	AC61	584,764	2,197,223
AC36	590,135	2,202,795				ACF141	586,060	2,209,753			

References

Acocella, V., Funiciello, R., 1999. The interaction between regional and local tectonics dur-ing resurgent doming: the case of the island of Ischia, Italy. J. Volcanol. Geotherm. Res. 88 (1–2), 109–123. https://doi.org/10.1016/S0377-0273(98)00109-7.

Acocella, V., Salvini, F., Funiciello, R., Faccenna, C., 1999. The role of transfer structures on volcanic activity at Campi Flegrei (Southern Italy). J. Volcanol. Geotherm. Res. 91, 123–139. https://doi.org/10.1016/s0377-0273(99)00032-3.

Acocella, V., Korme, T., Salvini, F., Funiciello, R., 2002. Elliptic calderas in the Ethiopian Rift: the control of pre-existing structures. J. Volcanol. Geotherm. Res. 119, 189–203.

Alsop, G.I., Marco, S., 2011. Soft-sediment deformation within seismogenic slumps of the Dead Sea Basin. J. Struct. Geol. 33, 433–457. https://doi.org/10.1016/j.jsg.2011.02.003.

Alsop, G.I., Weinberger, R., Marco, S., Levi, T., 2022. Criteria to identify sedimentary sills intruded during deformation of lacustrine sequences. J. Struct. Geol. 160, 104633 https://doi.org/10.1016/j.jsg.2022.104633.

Andersen, K.K., Azuma, N., Barnola, J.M., Bigler, M., Biscaye, P., Caillon, N., et al., 2004. High-resolution record of Northern Hemisphere climate extending into the last interglacial period. Nature 431 (7005), 147–151.

Angelier, J., 1979. Determination of the mean principal directions of stresses for a given fault population. Tectonophysics 56, 17–26.

Avellán, D.R., Macías, J.L., Layer, P.W., Cisneros, G., Sánchez- Núñez, J.M., Gómez-Vasconcelos, M.G., Pola, A., Sosa-Ceballos, G., García-Tenorio, F., Agustín, G.R., Osorio-Ocampo, S., García-Sánchez, L., Mendiola, I.M., Marti, J., López-Loera, H., Benowitz, J., 2019. Geology of the late Pliocene–Pleistocene Acoculco caldera complex, eastern Trans-Mexican Volcanic Belt (México). J. Maps 15 (2), 8–18. https://doi.org/10.1080/17445647.2018.1531075.

Avellán, D.R., Macías, J.L., Layer, P.W., Sosa-Ceballos, G., Gómez-Vasconcelos, M.G., Cisneros-Máximo, G., Sánchez-Núñez, J.M., Martí, J., García-Tenorio, F., López-Loera, A.P., Benowitz, J., 2020. Eruptive chronology of the Acoculco caldera complex – a resurgent caldera in the eastern Trans-Mexican Volcanic Belt (México). J. S. Am. Earth Sci. 98, 102412.

Barbier, E., 2002. Geothermal energy technology and current status: an overview. Renew. Sust. Energ. Rev. 6, 3–65.

Bolós, X., Del Ángel, V., Villanueva-Estrada, R.E., Sosa-Ceballos, G., Boijseauneau-López, M., Méndez, V., Macías, J.L., 2022. Surface hydrothermal activity controlled by the active structural system in the self-sealing geothermal field of Acoculco (Mexico). Geothermics 101, 102372. https://doi.org/10.1016/j.geothermics.2022.102372.

Brogi, A., Alçiçek, M.C., Liotta, D., Capezzuoli, E., Zucchi, M., Matera, P.F., 2021. Step-over fault zones controlling geothermal fluid-flow and travertine formation (Denizli Basin, Turkey). Geothermics 89, 101941. https://doi.org/10.1016/j.geothermics.2020.101941.

Canet, C., Arana, L., González-Partida, E., Pi, T., Prol-Ledesma, R.M., Franco, S.I., Villanueva- Estrada, R.E., Camprubí, A., Ramírez-Silva, G., López-Hernández, A., 2010. A statistics- based method for the short-wave infrared spectral analysis of altered rocks: an example from the Acoculco Caldera, Eastern Trans-Mexican Volcanic Belt. J. Geochem. Explor. 105, 1–10.

Canet, C., Hernández-Cruz, B., Jiménez-Franco, A., Pi, T., Peláez, B., Villanueva-Estrada, R.E., Salinas, S., 2015. Combining ammonium mapping and short-wave infrared (SWIR) reflectance spectroscopy to constrain a model of hydrothermal alteration for the Acoculco geothermal zone, Eastern México. Geothermics 53, 154–165.

Chavez-Ceballos, G., Torres-Ramos, J.A., Porras-Vasquez, N.D., Cossio-Torres, T., Aranda-Gomez, J.J., 2011. Evolución estructural del frente tectónico de la Sierra Madre Oriental en el Cañón Santa Rosa, Linares, Nuevo León. Bol. Soc. Geol. Mex. 63 (2), 253–270.

Córdoba-Montiel, F., Sieron, K., Iglesias, A., Caló, M., Artola, O.A.C., Alarcón, M.Á.M., Puente, L.F.R., 2023. New constraints on the seismotectonics and crustal structure of the Eastern Trans-Mexican Volcanic Belt based on local seismicity, focal mechanisms and a preliminary state of stress evaluation. J. S. Am. Earth Sci. 123, 104226 https://doi.org/10.1016/j.jsames.2023.104226.

Cuéllar-Cárdenas, M.A., Nieto-Samaniego, Á.F., Levresse, G., Alaniz-Álvarez, S.A., Solari, L., Ortega- Obregón, C., López-Martínez, M., 2012. Límites temporales de la deformación por acortamiento Laramide en el centro de México. Revista Mexicana de Ciencias Geológicas 29 (1) (179–2).

Curewitz, D., Karson, J.A., 1997. Structural settings of hydrothermal outflow: fracture permeability maintained by fault propagation and interaction. J. Volcanol. Geotherm. Res. 79, 149–168. https://doi.org/10.1016/S0377-0273(97)00027-00029.

Dansgaard, W., Johnsen, S.J., Clausen, H.B., Dahl-Jensen, D., Gundes-trup, N.S., Hammer, C.U., Hvidberg, C.S., Steffensen, J.P., Svein-bjornsdottir, A.E., Jouzel, J., Bond, G., 1993. Evidence for general instability of past climate from a 250-kyr ice-core record. Nature 364, 218–220.

De la Cruz, M.V., Castillo-Hernández, D., 1986. Estudio geológico de la zona geotérmica de la caldera de Acoculco, Puebla. CFE-GPG Internal report 36/86 (23 p).

Demant, A., Robin, C., 1975. Las fases del vulcanismo en México; una síntesis en relación con la evolución geodinamica desde el Cretácico. Revista Inst.Geol 75 (1), 66–79.

Dini, A., Westerman, D.S., Innocenti, F., Rocchi, S., 2008. Magma Emplacement in a Transfer Zone: the Miocene Mafic Orano Dyke Swarm of Elba. In: Island, 302. Geological Society London Special Publications, Tuscany, Italy, pp. 131–148.

Ego, F., Ansan, V., 2002. Why is the Central Trans-Mexican Volcanic Belt (102°–99°W) in transtensive deformation? Tectonophysics 359, 189–208.

Eguiluz de Antuñano, S., Aranda-García, M., Marren, R., 2000. Tectónica de la Sierra Madre Oriental, Mexico. Bol. Soc. Geol. Mex. 53, 1–26.

Esquivel-Mendiola, L.I., Calò, M., Tramelli, A., Figueroa-Soto, A., 2022. Optimization of local scale seismic networks applied to geothermal fields. The case of the Acoculco caldera, Mexico. J. S. Am. Earth Sci. 119, 103995 https://doi.org/10.1016/j.jsames.2022.103995.

Faulds, J.E., Coolbaugh, M.F., Hinz, N.H., Cashman, P.H., Kratt, C., Dering, G., Edwards, J., Mayhew, B., McLachlan, H., 2011. Assessment of favorable structural settings of geothermal systems in the Great Basin, western USA. Geotherm. Resour. Council Transact. 35, 777–784.

Faulkner, D.R., Armitage, P.J., 2013. The effect of tectonic environment on permeability development around faults and in the brittle crust. Earth Planet. Sci. Lett. 375, 71–77.

Ferguson, J.F., Cogbill, A.H., Warren, R.G., 1994. A geophysical-geological transect of the Silent Canyon Caldera complex, Pahute Mesa, Nevada. J. Geophys. Res. Solid Earth 99, 4323–4339. https://doi.org/10.1029/93jb02447.

Ferrari, L., Pasquare, G., Venegas-Salgado, S., Romero-Rios, F., 1999. Geology of the Western Mexican Volcanic Belt and Adjacent Sierra Madre Occidental and Jalisco Block. Geological Society of America (Special Paper 334).

Ferrari, L., Conticelli, S., Vaggelli, G., Petrone, C.M., Maneo, P., 2000. Late Miocene volcanism and intra-arc tectonics during the early development of the Trans-Mexican Volcanic Belt. Tectonophysics 318, 161–185.

Ferrari, L., Orozco-Esquivel, T., Manea, V., Manea, M., 2011. The dynamic history of the Trans- Mexican Volcanic Belt and the Mexico subduction zone. Tectonophysics 522–523 (5), 122–149.

Fitz-Díaz, E., Tolson, G., Hudleston, P., Bolaños-Rodríguez, D., Ortega-Flores, B., Vásquez-Serrano, A., 2012. The role of folding in the development of the Mexican fold-and-thrust belt. Geosphere Geol. Soc. America 8 (4), 931–949.
Fitz-Diaz, E., Hudleston, P., Tolson, G., der Pluijm, Van, a, B., 2014. Progressive, episodic deformation in the Mexican Fold–Thrust Belt (central Mexico): evidence from isotopic dating of folds and faults. Int. Geol. Rev. 56 (6), 734–755.
Fossen, H., Rotevatn, A., 2016. Fault linkage and relay structures in extensional settings—a review. Earth Sci. Rev. 154, 14–28. https://doi.org/10.1016/j.earscirev.2015.11.014.
García-Palomo, A., Macías, J.L., Garduño-Monroy, V.H., 2000. Miocene to recent structural evolution of the Nevado de Toluca volcano region, Central Mexico. Tectonophysics 318, 281–302.
García-Palomo, A., Macías, J.L., Tolson, G., Valdez, G., Mora, J.C., 2002a. Volcanic stratigraphy and geological evolution of the Apan región, east-central sector of the Trans-Mexican Volcanic Belt. Geofis. Int. 41, 133–150.
García-Palomo, A., Macías, J.L., Tolson, G., Valdez, G., Mora, J.C., 2002b. Volcanic straHgraphy and geological evolution of the Apan region, east-central sector of the Trans-Mexican Volcanic Belt. Geofis. Int. 41 (2), 133–150.
García-Palomo, A., Macías, J.L., Jiménez, A., Tolson, G., Mena, M., Sánchez-Núñez, J.M., Arce, J.L., Layer, P.W., Santoyo, M.A., Lermo-Samaniego, J., 2018. NW-SE Pliocene-Quaternary extension in the Apan-Acoculco region, eastern Trans-Mexican Volcanic Belt. J. Volcanol. Geotherm. Res. 349 (1), 240–255.
Garduño-Monroy, V.H., Gutiérrez-Negrín, L.C.A., 1992. Magmatismo, hiatus y tectonismo de la Sierra Madre Occidental y del Cinturón Volcánico Mexicano. Geofis. Int. 31 (4), 417–429.
Garduño-Monroy, V.H., Spinnler, J., Ceragioli, E., 1993. Geological and structural study of the Chapala rift, State of Jalisco, Mexico. Geofis. Int. 32 (3), 487–499.
Gómez-Alvarez, F., Garduño-Monroy, V.H., Sosa-Ceballos, G., Jiménez-Haro, A., Liotta, D., Gaitan-Ramirez, M.F., Brogi, A., Israde-Alcántara, I., Najera-Blas, S.M., Wheeler, W., Forster, M., Garcia-Hernández, O.H., 2021. New constraints on tectonism and magmatism from the eastern sector of the Trans-Mexican Volcanic Belt (Chignahuapan Horst, Puebla, México). J. S. Am. Earth Sci. 112 (Part 1) https://doi.org/10.1016/j.jsames.2021.103468.
Gómez-Tuena, A., Orozco-Esquivel, M.T., Ferrari, L., 2005. Petrogénesis ígnea de la Faja Volcánica Transmexicana. Boletín de la Sociedad Geológica Mexicana. Volumen Conmemorativo del Centenario. Temas Selectos de la Geología Mexicana 57 (3), 227–283.
Gómez-Vasconcelos, M.G., Garduño-Monroy, V.H., Macías, J.L., Layer, P.W., Benowitz, J. A., 2015. The Sierra de Mil Cumbres, Michoacán, México: Transitional volcanism between the Sierra Madre Occidental and the Trans-Mexican Volcanic Belt. J. Volcanol. Geotherm. Res. 301, 128–147.
Gutiérrez-Negrín, L.C.A., 2013. Evolución del sistema geotérmico de Acoculco, Pue., México: un estudio con base en estudios petrográficos del pozo EAC-2 y en otras consideraciones. Geotermia 24 (1), 14–24.
Hasenaka, T., 1994. Size, distribution, and magma output rate for shield vol-canoes of the Michoacan-Guanajuato volcanic field Central Mexico. J. Volcanol. Geotherm. Res. 63, 13–31.
Kim, Y.-S., Peacock, D.C.P., Sanderson, D.J., 2004. Fault damage zones. J. Struct. Geol. 26, 503–517. https://doi.org/10.1016/j.jsg.2003.08.002.
Knipe, R.J., 1986. Deformation mechanism path diagrams for sediments undergoing lithification. Mem. Geol. Soc. Am. 166, 151–160.
Lermo-Samaniego, J., Bernal-Esquia, I., 2006. Boletín de la Sociedad Geológica Mexicana. Número Especial de Geología Urbana 58 (2), 215–221. https://doi.org/10.18268/BSGM2006v58n2a8.
Liotta, D., Brogi, A., 2020. Pliocene-Quaternary fault kinematics in the Larderello geothermal area (Italy): insights for the interpretation of the present stress field. Geothermics 83, 101714. https://doi.org/10.1016/j.geothermics.2019.101714.
Liotta, D., Brogi, A., Meccheri, M., Dini, A., Bianco, C., Ruggieri, G., 2015. Coexistence of low-angle normal and high-angle strike- to oblique-slip faults during Late Miocene mineralization in eastern Elba Island (Italy). Tectonophysics 660, 17–34.
Lopez-Hernandez, A., Castillo-Hernandez, D., 1997. Exploratory drilling at Acoculco, Puebla, Mexico: a hydrothermal system with only non thermal manifestations. Geotherm. Resour. Council Transact. 21, 429–433.
López-Hernández, A., Martínez, E.I., 1996. Evaluación vulcanológica y estructural de la zona geotérmica de Acoculco, Puebla, y su relación con la anomalía termal detectada en el pozo EAC-1 (Internal Report OGL-AC- 11/96). CFE-GPG, México.
López-Hernández, A., García-Estrada, G., Aguirre-Díaz, G., González-Partida, E., Palma-Guzmán, H., Quijano-León, J.L., 2009. Hydrothermal activity in the Tulancingo–Acoculco Caldera Complex, central Mexico: Exploratory studies. Geothermics 38 (3), 279–293. https://doi.org/10.1016/j.geothermics.2009.05.001.
Lorenzo-Pulido, C., Flores-Armenta, M., Ramírez-Silva, G., 2011. Caracterización de un yacimiento de roca seca caliente en la zona geotérmica de Acoculco, Pue. Geotermia 24 (1), 59–69.
Maestrelli, D., Bonini, M., Corti, G., Del Ventisette, C., Moratti, G., Montanari, D., 2021. Exploring fault propagation and the role of inherited structures during caldera collapse through laboratory experiments. J. Volcanol. Geotherm. Res. 414, 107232 https://doi.org/10.1016/j.jvolgeores.2021.107232.
Mathieu, L., Vries, B., Pilato, M., Troll, V.R., 2011. The interaction between volcanoes and strike-slip, transtensional and transpressional fault zones: Analogue models and natural examples. J. Struct. Geol. 33, 898–906. https://doi.org/10.1016/j.jsg.2011.03.003.
Micklethwaite, S., Ford, A., Witt, W., Sheldon, H.A., 2015. The where and how of faults, fluids and permeability - insights from fault stepovers, scaling properties and gold mineralization. Geofluids 15, 240–251. https://doi.org/10.1111/gfl.12102.
Milner, D., Cole, J., Wood, C., 2002. Asymmetric, multiple-block collapse at Rotorua Caldera, Taupo volcanic zone, New Zealand. Bull. Volcanol. 64 (2), 134–149. https://doi.org/10.1007/s00445-001-0191-0.
Olvera-García, E., Garduño-Monroy, V.H., Liotta, L., Brogi, A., Bermejo-Santoyo, G., Guevara-Alday, J.A., 2020. Neogene-Quaternary normal and transfer faults controlling deep-seated geothermal systems: the case of San Agustín del Maíz (central Trans-Mexican Volcanic Belt, México). Geothermics 86, 101791.
Padilla-Sanchez, R.J., 2007. Evolución geológica del sureste mexicano desde el Mesozoico al presente en el contexto regional del Golfo de México. Bol. Soc. Geol. Mex. 59, 19–42.
Palladino, G., Alsop, G.I., Grippa, A., Zvirtes, G., Phillip, R.P., Hurst, A., 2018. Sandstone filled normal faults: a case study from Central California. J. Struct. Geol. 110, 86–101.
Palladino, G., Rizzo, R.E., Zvirtes, G., Grippa, A., Phillip, R.P., Healy, D., Alsop, G.I., 2020. Multiple episodes of sand injection leading to accumulation and leakage of hydrocarbons along the San Andreas/San Gregorio fault system, California. Mar. Pet. Geol. 118, 104431.
Pasquaré, G., Garduño, V.H., Tibaldi, A., Tectonophysics, M.F., 1988. Stress pattern evolution in the central sector of the Mexican Volcanic Belt. Tectonophysics 146, 353–364.
Pasquaré, G., Ferrari, L., Garduño-Monroy, V.H., Tibaldi, A., Vezzoli, L., 1991. Geologic map of the central sector of the Mexican Volcanic Belt, states of Guanajuato and Michoacán. In: Geological Society of America. Map and Chart Series MCH072.
Peacock, D.C.P., Sanderson, D.J., 1991. Displacements, segment linkage and relay ramps in normal fault zones. J. Struct. Geol. 13, 721–733.
Peiffer, L., Bernard-Romero, R., Mazot, A., Taran, Y.A., Guevara, M., Santoyo, E., 2014. Fluidgeochemistry and soil gas fluxes (CO2–CH4–H2S) at a promissory hot dry rock geo-thermal system: the Acoculco caldera, México. J. Volcanol. Geotherm. Res. 284, 122–137.
Pérez-Flores, P., Cembrano, J., Sánchez-Alfaro, P., Veloso, E., Arancibia, G., Roquer, T., 2016. Tectonics, magmatism and paleo-fluid distribution in a strike-slip setting: Insights from the northern termination of the Liquiñe–Ofqui fault System, Chile. Tectonophysics 680, 192–210. https://doi.org/10.1016/j.tecto.2016.05.016.
Pérez-Orozco, J.D., Sosa-Ceballos, G., Lithos, J.M., 2021. Tectonic and magmatic controls on the evolution of post-collapse volcanism. Insights from the Acoculco Caldera Complex, Puebla, México. Lithos 380–381 (2021), 105878. https://doi.org/10.1016/j.lithos.2020.105878.
Perton, M., Hernández, L.T.M., Figueroa-Soto, A., Sosa-Ceballos, G., Amador, J.D.J., Angulo, J., Calò, M., 2022. The magmatic plumbing system of the Acoculco volcanic complex (Mexico) revealed by ambient noise tomography. J. Volcanol. Geotherm. Res. 432, 107704 https://doi.org/10.1016/j.jvolgeores.2022.107704.
Petrinovic, I.A., Martí, J., Aguirre-Díaz, G.J., Guzmán, S., Geyer, A., Paz, N.S., 2010. The Cerro Aguas Calientes caldera, NW Argentina: an example of a tectonically controlled, polygenetic collapse caldera, and its regional significance. J. Volcanol. Geotherm. Res. 194, 15–26. https://doi.org/10.1016/j.jvolgeores.2010.04.012.
Polak, B.G., Prasalov, E.M., Kononov, V.I., Verkovsky, A.B., González, A., Templos, L.A., Espíndola, J.M., Arellano, J.M., Mañón, A., 1982. Isotopic composition and concentration of inert gases in Mexican hydrothermal systems. Geofis. Int. 21, 193–227.
Prol-Ledesma, R.M., Morán-Zenteno, D.J., 2019. Heat flow and geothermal provinces in Mexico. Geothermics 78, 183–200. https://doi.org/10.1016/j.geothermics.2018.12.009.
Quintanar, L., Rodríguez-González, M., Campos-Enríquez, O., 2004. A shallow crustal earthquake doublet from the Trans-Mexican Volcanic Belt (Central Mexico). Bull. Seism. Soc. America 94, 845–855.
Quintanar, L., Cárdenas-Ramírez, A., Bello-Segura, D.I., Espíndola, V.H., Pérez-Santana, J.A., Cárdenas-Monroy, C., Carmona-Gallegos, A.L., Rodríguez-Rasilla, I., 2018. A seismic network for the Valley of Mexico: present status and perspectives. Seismol. Res. Lett. 89 (2A), 356–362.
Quinto, A., Santoyo, E., Torres, V., González, E., Castillo, H.D., 1995. Estudio geoquímico-ambiental de los efluentes naturales producidos en la zona geotérmica de Acoculco. Puebla. Ingeniería Hidráulica en México X 3, 21–27.
Román Fernández, B., 2018. Relación de las descargas hidrotermales superficiales y el sistema estructural en la Caldera de Acoculco Puebla. Tesis de Maestría. Instituto de Investigaciones en Ciencias de la Tierra. Universidad Michoacana de San Nicolás de Hidalgo.
Rowland, J., Sibson, R.H., 2004. Structural controls on hydrothermal flow in a segmented rift system, Taupo Volcanic Zone, New Zealand. Geofluids 4, 259–283.
Sedlock, R.L., Ortega-Gutierrez, F., Speed, R.C., 1993. Tectonostratigraphic terranes and tectonic evolution of Mexico. Geol. Soc. Am. Spec. Pap. 278 (153 pages).
Seebeck, H., Nicol, A., Walsh, J.J., Childs, C., Beetham, R.D., Pettinga, J., 2014. Fluid flow in fault zones from an active rift. J. Struct. Geol. 62, 52–64. https://doi.org/10.1016/j.jsg.2014.01.008.
Sibson, R.H., 2000. Fluid involvement in normal faulting. J. Geodyn. 29, 469–499.
Sosa-Ceballos, G., Macías, J.L., Avellán, D.R., Salazar-Hermenegildo, N., Boijseauneau-López, M.E., Pérez-Orozco, J.D., 2018. The Acoculco Caldera complex magmas: Genesis, evolution and relation with the Acoculco geothermal system. J. Volcanol. Geotherm. Res. 358, 288–306.
Suter, M., 1991. State of stress and active deformation in Mexico andwestern Central America. In: Slemmons, D.B. (Ed.), Neotectonics of North America, 1. Geological Society of America, Boulder,Colorado, Decade Map, pp. 401–1421.
Suárez, G., Caballero-Jiménez, G.V., Novelo-Casanova, D.A., 2019. Active crustal deformation in the TransáMexican Volcanic Belt as evidenced by historical earthquakes during the last 450 years. Tectonics 38, 1–19.
Suter, M., 1987. Structural traverse across the Sierra Madre oriental fold-thrust belt in east-Central Mexico. Geol. Soc. Am. Boll. 98, 249–264.

Suter, M., Lopéz-Martínez, M., Quintero-Legorreta, O., Carrillo-Marinez, M., 2001. Quaternary intra-arc extension in the central Trans-Mexican volcanic belt. Bol. Soc. Geol. Mex. 113, 693–703.

Vega, R.C., Flores, V.T., Fleites, G.L., Montalvo, A.C., 2014. Agresividad de las precipitaciones en la subcuenca del río San Marcos, Puebla, México. Investig. Geográficas 83, 28–40.

Viggiano-Guerra, J.C., Flores-Armenta, M., Ramírez-Silva, G.R., 2011. Evolución del sistema geotérmico de Acoculco, Puebla, México: un estudio con base en estudios petrográficos del pozo EAC-2 y en otras consideraciones. Geotermia: Revista Mexicana de Geoenergía 24, 14–24.

Waldron, J.W.F., Gagnon, J.F., 2011. Recognizing soft-sediment structures in deformed rocks of orogens. J. Struct. Geol. 33, 271–279. https://doi.org/10.1016/j.jsg.2010.06.015.